

Neglecting the effect of long- and short-term erosion can lead to spurious coastal flood risk projections and maladaptation

A. Toimil^{*}, M. Álvarez-Cuesta, I.J. Losada

IHCantabria - Instituto de Hidráulica Ambiental de la Universidad de Cantabria, Isabel Torres 15, 39011, Santander, Spain



ABSTRACT

Flooding and erosion are among the most relevant hazards for coastal regions and although they are linked, their inherent complexity has typically led them to be addressed separately, potentially leading to highly uncertain estimates. This paper has three aims: (a) to present a methodology for coupling coastal flood projections with shoreline changes; (b) to quantify the effects of neglecting the coupling of flooding and erosion on future projections at a case study location; and (c) to analyse the relative importance of the climate-related uncertainty sources. We use a suite of statistical, process-based, and physics-based models to generate and downscale storms, compute water levels affected by storm morphodynamics and long-term profile changes and propagate flooding over topo-bathymetries that are in turn modified to incorporate the impact of sea-level rise, longshore sediment transport and storm-driven erosion. We sample climate uncertainty by considering storm variability (synthetic generation) and ensembles of radiative forcing scenarios, regional climate models, and sea-level rise trajectories. For illustration purposes, we consider a 40-km coastal stretch in the Spanish Mediterranean. We find that if the effect of erosion is neglected, the mean values of the total water level and flooded area can be either over- or underestimated by up to 18% and 22%, and up to 7% and 85%, respectively, with respect to our coupled results. The factors that most influence total water levels are storm erosion and profile geometry, highlighting the relevance of using real profiles in shoreface translation. In the flooded area, longshore transport can play a fundamental enhancing role. We also find that the coupling approach used can contribute more to the projection of flooded areas than the choice of climate models and sea-level rise trajectories even by 2100 (up to 76% versus 8% and 16%, respectively). We conclude that neglecting erosion effects on coastal flooding can have management implications, especially for urban beaches, leading to poor adaptation planning and maladaptation.

1. Introduction

Climate change is and will continue to increase mean sea level (Fox-Kemper et al., 2021) and alter the frequency of extreme waves and storm surges (Lobeto et al., 2021; Tebaldi et al., 2021), hence posing growing risks to coastal areas and exacerbating the problems these regions already face (Wong et al., 2014; Collins et al., 2019). On developed coasts with fixed low-elevation infrastructure and real estate, one of these key problems is coastal flooding, which results from the superposition of individual but interacting (compound or cascading) hydrodynamic and morphologic processes at different scales (Toimil et al., 2020a). They include the effect of nearshore bathymetry on surf-zone coastal dynamics and the influence of long-term shoreface and storm erosion on flood extent and depth over the ground (Pollard et al., 2019). Beach retreat can lead to more exceptional coastal flooding and cause its consequences to reach levels of scale greater than would have been caused by flooding in isolation. These factors are likely to change over time, as are their interactions, which are increasingly complex and uncertain but cannot be neglected in the development of coastal flood projections.

Although the literature recognises the importance of modelling coastal flooding and erosion together (e.g., Lentz et al., 2016; Barnard et al., 2019; Pollard et al., 2019; Leaman et al., 2021), most studies to date continue to consider these two impacts separately because their coupling is not straightforward. One main challenge comes from the time scale problem, as flooding and erosion occur at different time scales. These time scales are related to their driving forcing conditions and are likely to be altered by climate change (Ranasinghe, 2016; Toimil et al., 2020b). At the storm scale (hours to days), extreme weather events due to storm surges and waves are the main drivers of both episodic flooding and the erosion of dunes and beaches. These events are expected to increase in frequency mostly due to sea-level rise (SLR) and are likely to change in intensity due to the effects of climate change, resulting in more storm impacts and potential variations in flood severity and erosion rates. Embayed beaches rotate due to alongshore transport as waves approach the coast at an angle; therefore, in the medium term (months to years), changes in mean wave direction could drive continued erosion or accretion and alter the beach planform, potentially leading to inundation in some areas. Finally, at longer time scales (years to decades), SLR will induce permanent lowland

* Corresponding author.

E-mail address: toimila@unican.es (A. Toimil).

inundation and shoreline recession (Nicholls and Cazenave, 2010; Cazenave and Le Cozannet, 2013). Higher water levels will allow wave erosion processes to act farther up on the beach profile causing a readjustment that will result in net beach erosion and deposition on the nearshore bottom (Bruun, 1962). Deeper water will decrease wave refraction and increase the capacity for alongshore transport, allowing waves to get closer to the shoreface before breaking and causing increased flooding. Sustained and/or chronic shoreline recession will likewise imply the loss of natural flood defences. For these reasons, where highly accurate flood maps are required (e.g., to make decisions on coastal adaptation), present-day topo-bathymetric data (topobathy, hereinafter) need to be corrected to account for potential climate change-driven storm erosion and shoreline changes (Barnard et al., 2019).

In addition to the time scale problem, the spatial scale required for coastal adaptation decisions may span from tens to hundreds of kilometres and that contemporary risk-based planning frameworks demand an appropriate uncertainty characterisation of impact estimates, which usually involve running the impact model many times (Ranasinghe, 2016). Within this context (~10 km–~100 km, days to centuries, and sufficient uncertainty treatment), the joint modelling of coastal flooding and erosion projections would ideally require an efficient multi-scale coastal impact model that concurrently simulates the different physical processes involved in projected coastal flooding and erosion and their interaction at distinct spatio-temporal scales, including inter-scale morphodynamics. However, this model is not yet available, as current process-based models do not allow addressing all relevant scales (Toimil et al., 2020a). Computational constraints and calibration requirements often limit their application to O(10 km) (Sherwood et al., 2022); and simulations that exceed the storm scale may produce meaningless results due to the accumulation of knowledge uncertainties and numerical errors (Splinter and Coco, 2021; Vitousek et al., 2017a). Therefore, until computational resources and our knowledge of processes enable the development of this single multi-scale model, approaches that rely on impact model chains (e.g., Barnard et al., 2019) integrating process-based models (solving hydro-and morphodynamics interactions), physics-based models (solving single-dominant physical processes) and statistical tools can offer a trade-off between efficiency and accuracy at the time and spatial scales required.

When it comes to modelling the erosion-flooding chain, one of the most critical aspects is the prediction of long-term coastline changes. Complex process-based models are well-suited for modelling storm erosion, but at present they are still not capable of providing reliable predictions of shoreline change considering uncertainty beyond just a few years (Ranasinghe, 2020). Reduced-complexity models, such as shoreline evolution models, are the preferred choice to reproduce seasonal to multi-annual shoreline change oscillations (Vitousek et al., 2017b; Antolínez et al., 2019; Álvarez-Cuesta et al., 2021b). These models are efficient, so they can be used to simulate multiple future climate scenarios but can have limitations when applied outside the regime of calibration (Montaño et al., 2020). For longer time scales, this is further complicated by the lack of long-term, large-scale monitoring of sandy beaches (Splinter and Coco, 2021), the difficulties in incorporating the effect of SLR in a robust manner (Vitousek et al., 2017a), and the uncertainty in climate forcing that increases with time and cannot be ignored (Toimil et al., 2021).

As hereinafter described in our state-of-the-art review, the spatio-temporal scale of the coupled erosion-flooding problem highly conditions the type of models to be used. For forensic event-scale studies and storm impact projections, process-based models are the most widely applied. However, when it comes to consider long-term shoreline changes, current approaches mainly rely on the combination of simpler and more efficient methods such as trend extrapolation, rules-based morphodynamic update, reduced-complexity modelling and statistical techniques.

Several studies focused on storm-induced dune erosion, breaching

and overwash at local and regional scales have been published. McCall et al. (2010) applied XBeach (Roelvink et al., 2009) to simulate 2DH overwash morphology on a portion of a barrier island, Santa Rosa Island (Florida), during Hurricane Ivan (2004). More recently, Gharagozlou et al. (2020) used XBeach to reproduce morphodynamics, overwash, and inundation during Hurricane Isabel (2003) in the North Carolina Outer Banks. The authors found that even when using a fixed topography in a regional ocean model (ADCIRC, Luettich et al., 1992), flood predictions improved significantly when post-storm topography from XBeach was considered. Similarly, Van Ormondt et al. (2020) ran XBeach to hindcast the morphodynamic evolution of a breach on eastern Fire Island (New York) over the first 3 years after its formation during Hurricane Sandy (2012). XBeach 2DH was also utilised by Passeri et al. (2018) and Grases et al. (2020) in the context of climate change. Passeri et al. (2018) simulated the hydrodynamic and morphodynamic impacts of hurricanes Ivan (2004) and Katrina (2005) on Dauphin Island under present-day and future sea levels. Grases et al. (2020) examined the interaction of beach morphology with current and future storms at the local scale in Riumar (Ebro Delta, Spain). To simulate dune erosion, overwash and inundation in 2050 and 2100, the authors combined the representative concentration pathway (RCP) RCP8.5 SLR 90th percentile with a set of future storms obtained from the synthetic emulation of Lin-Ye et al. (2017), which was performed under a stationary climate assumption. Another recent application of XBeach 2DH comes from Sanuy and Jimenez (2021), who proposed a response-based approach (Sanuy et al., 2019) to model bed-level changes and coastal flooding related to 179 storms in the Tordera Delta (Spain). The authors modified the topobathy by moving the active part of the shoreface landwards to consider erosion rates extrapolated 5, 10 and 20 years into the future. McCall et al. (2010), Gharagozlou et al. (2020) and Van Ormondt et al. (2020) provide examples of forensic studies where pre- and post-storm topobathy were at hand, allowing the model skill to reproduce changes in breach geometry, volume changes and flood extent. Sanuy and Jimenez (2021) did not include climate change effects but did generate storms with a certain degree of probabilistic development (using Bayesian networks), updating the topobathy to account for medium-term erosion derived from trend analysis. Conversely, Passeri et al. (2018) and Grases et al. (2020) did consider climate change, although only through two and one SLR scenarios, respectively. Furthermore, none of them updated the topobathy to account for long-term shoreline change, and climate-related uncertainty sampling was very limited in both cases.

Moving to studies that account for long-term shoreline changes in coastal flooding, Benavente et al. (2006) implemented a flood extent model for two types of storms in Valdelagran spit and marshes (Spain). The authors calculated theoretical storm elevations and corrected the topography using rates of shoreline change obtained from aerial photographs. They found that long-term coastline retreat trends represent an important factor in the prediction of coastal flooding, as they can increase exposure to sea storms. More recently, Stripling et al. (2017) proposed UnaLinea, a one-line model for simulating shoreline evolution. The model was applied deterministically to the west coast of Calabria (Italy) and probabilistically to an idealised coastal stretch of the Holderness (UK). In the latter case, UnaLinea estimates allowed for the RASP-SU model (Gouldby et al., 2010) to adjust seawall toe levels and calculate overtopping rates to be used to force a 2D flood model (RFSM, Gouldby et al., 2008), yielding storm-induced flood maps. Benavente et al. (2006) and Stripling et al. (2017) did not incorporate the effects of climate change, but other studies did. For instance, Dawson et al. (2009) developed a methodology to integrate shoreline changes into coastal flood projections for the twenty-first century on the East Anglian coast (UK). The authors connected coastal flooding and erosion by introducing changes in the shoreline position (modelled with SCAPE, Walkden and Hall, 2005) into the probability of failure of flood defence structures rather than in the topography used to model flooding (with LISFLOOD-FP, Bates and De Roo, 2000). Strictly speaking, climate change was incorporated in terms of SLR, and climate-related

uncertainty sampling was limited to considering different SLR scenarios and undertaking a sensitivity analysis of wave height and direction changes. A few years later, Passeri et al. (2015, 2016) examined the influence of incorporating long-term shoreline changes into hydrodynamic modelling and inundation along the northern Gulf of Mexico under future SLR scenarios. In the first case, the authors considered the impact of several hurricanes and a single SLR scenario; in the second, they evaluated variations in tidal amplitudes for different SLR scenarios and projected future shoreline changes and dune heights using a Bayesian network model (Gutierrez et al., 2014), of which the 50th percentile was selected to represent an average projection of future morphology. In both studies, beach profiles were translated upwards by the amount of SLR and landwards/seawards by the amount of projected erosion/accretion while maintaining shape.

Nearly a decade later, Grilli et al. (2017) assessed coastal flood risks in Charlestown (Rhode Island) associated with the 100-year storm, including the effects of SLR (range of values) and dune erosion. The authors updated the topography by replacing the current dune profile with an empirical storm profile and by shifting it landwards and upwards to account for episodic dune erosion and long-term shoreline retreat, respectively. Flood maps were obtained using a static inundation method based on GIS interpolation. Finally, within the framework of the CoSMoS (Coastal Storm Modeling System) Project, Barnard et al. (2019) presented a modelling approach to estimate climate change-driven changes in coastal flood exposure along the coast of California. Global climate model (GCM)-driven projections were used as boundary conditions for a suite of oceanographic, hydrodynamic, and geomorphic models to predict coastal waves, water levels, flooding, and erosion for different SLR and storm scenarios over the 21st century. Projected long-term estimates of shoreline change (modelled with the CoSMoS-COAST model, Vitousek et al., 2017b) and cliff retreat (Limber et al., 2018) were employed to translate cross-shore profiles extracted from a digital elevation model upwards and landwards (Erikson et al., 2017). The authors used the evolved profiles as the basis for the bathtub method forced with 1D XBeach-derived dynamics to provide flood maps for the scenarios considered. Despite the comprehensiveness of the approach, uncertainty sampling is very limited both in terms of the dynamics used (range of SLR values but wave projections associated with a single GCM and RCP) and in its statistical treatment (storms are obtained directly from the projected wave time series). Additionally, static inundation methods that do not account for flood dynamics and could be inaccurate (Menendez et al., 2019).

In this paper, we propose a methodology to advance projections of coastal flooding coupled with coastal erosion at all the relevant scales at which these impacts interact, using surveyed profiles throughout the process. We quantify the influence of long-term profile displacements and storm morphodynamics on total water level (TWL) and the combined effect of such TWL estimates with long-term shoreface translation and storm-driven beach erosion on the flooded area. To analyse the importance of the flood-erosion coupling, we compare the outcomes of the fully coupled approach with those of two simplifications (only short- or long-term coupling) and the traditional approach of no coupling at any scale. The methodology, which includes the application of a series of process- and physics-based models, has a strong climate-related uncertainty sampling component, as it considers future storm variability from different RCPs and regional climate models (RCMs) in combination with different SLR trajectories. Using 2005, 2050 and 2100 as target horizon years, we also evaluate the spread range of flood-related outcomes associated with different levels of flood-erosion coupling and their contribution to total uncertainty.

2. Materials and methods

2.1. Overview of the methodology and coupling approaches

The methodology that we propose to develop coastal flood

projections, including the effects of coastal erosion, is organised into 6 modules, as shown in Fig. 1. We first collect bias-corrected dynamically downscaled waves and storm surge projections (IHCantabria, 2020), SLR projections (Oppenheimer et al., 2019) and astronomical tides (Box 1). Hereafter, we proceed with the modelling of coastal flooding, where the updating of the topobathy in two phases plays a key role in incorporating shoreline changes at different time scales (i.e., short and/or long term). The second module is the modelling of probabilistic storms (Box 2). We generate thousands of synthetic multivariate storms by setting up and applying a statistical model that couples a multivariate model of extremes and a multivariate model of wave direction, allowing us to jointly consider the spatial dependence of climate forcing conditions and their non-stationarity. The third module (Box 3) consists of the hybrid (statistical-numerical) downscaling of storms and the calculation of TWL by adding wave and sea level components. We use clustering techniques, a wave propagation model (SWAN, Booij et al., 1999), a hydrodynamic model (XBeach, Roelvink et al., 2009), and a multidimensional interpolation method based on radial basis functions (RBFs) to propagate storms and numerically compute the associated wave contribution. Modules 3 and 4 (Box 3 and Box 4, respectively) are interrelated since after downscaling the storms, we incorporate long-term shoreface changes in the topobathy on which surf-zone hydrodynamics are to be modelled. We apply a shoreface translation model (ShoreTrans, McCarroll et al., 2021) to update beach profiles in response to long-term sediment-supply variations calculated with a shoreline evolution model of reduced calibration uncertainty (IH-LANS, Alvarez-Cuesta et al., 2021a) and SLR. Over the long-term modified profiles, we run XBeach with storm morphodynamics activated so short-term erosion also has an effect on the TWL. The fifth module (Box 5) comprises TWL extreme value probability fitting and hydraulic modelling. We derive statistically robust extreme TWL values on which SLR is superimposed and use them to force a 2D flood model with sub-element topography (RFSM-EDA, Jamieson et al., 2012). Module 5 is in turn connected to module 4 as we apply another functionality of ShoreTrans (based on the model of Kinsela et al., 2017) to further modify the already long-term updated topobathy to incorporate the effect of storm erosion that is derived from IH-LANS simulations. We use the resulting topobathy for the hydraulic propagation of TWL events over ground (coastal flooding). The main outputs of this methodology are extreme TWL values and coastal flood maps. The sequence of steps and their interrelationships are displayed in a cascading fashion in the left panel of Fig. 1. In the standard approach, the topobathy update does not apply, and in the two simplified approaches, only the long- or short-term topobathy update applies in each case.

The last module (Box 6) is cross-cutting and aims at sufficiently sampling the uncertainty cascade associated with the climate-related flood and erosion drivers considered. We use projections of waves and storm surges for 2 RCPs and 5 GCM-RCM configurations (for brevity, RCMs hereinafter). Both scenario and climate model uncertainty are inherited by the storms, which in turn account for thousands of potential realisations of projected waves and storm surges in combination with astronomical tides (denoted as storm uncertainty) and SLR. We sample SLR trajectory uncertainty by considering 3 SLR percentiles of the distribution of 20 climate models that also inherit scenario uncertainty. For the future topobathies, we model shoreline change estimates associated with the same projections of waves and storm surges, thus with the same 2 RCPs and 5 RCMs. Additionally, the shoreline evolution model used incorporates a data assimilation algorithm that helps reduce epistemic (knowledge-based) uncertainty.

To analyse the importance of coastal flooding and erosion coupling at different time scales, we compare the outcomes of the fully coupled approach (CA) with those of 2 simplifications and no CA, resulting in the application of 4 CAs that differ in the consideration of shoreface changes in the modelling of TWL and flooded area. These approaches are 1) full CA, which considers both short- and long-term shoreface changes; 2) short-term CA, which accounts for only short-term shoreface changes; 3)

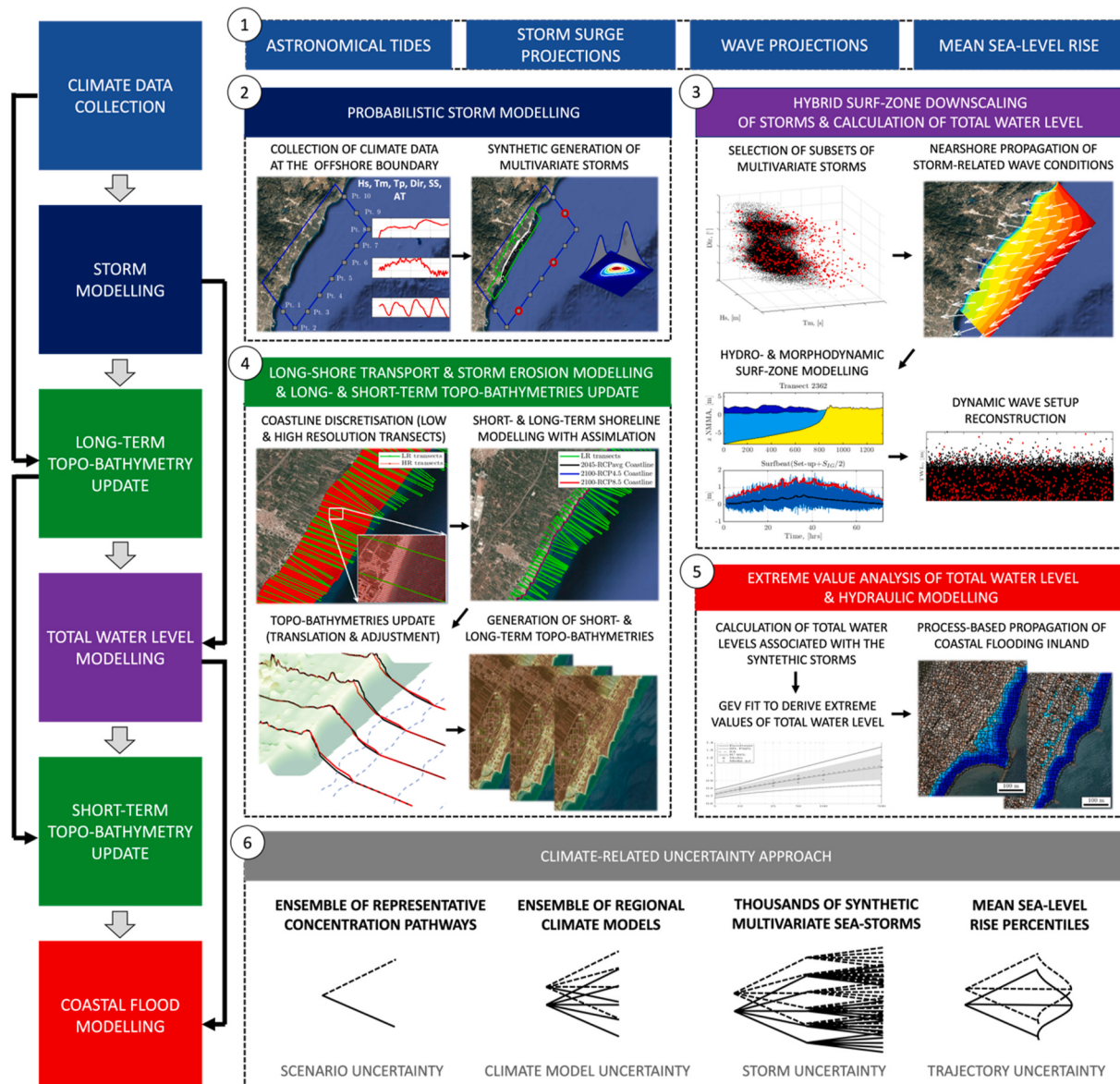


Fig. 1. Flowchart describing the methodology proposed for the development of coastal flood hazard projections incorporating shoreline change estimates. In the left-hand panel, the black arrows indicate input-output relationships between modules.

long-term CA, which is limited to considering the long-term shoreface response; and 4) no CA, in which the shoreface remains unchanged. While the no CA is the standard approach, especially in the context of the study of climate change impacts, the short-term CA applies mainly to forensic analyses (e.g., XBeach applications to simulate hydrodynamics and morphodynamics), and the long-term CA has mostly been used thus far to consider the effect of shoreline-change trends and SLR on topography.

Each CA requires the application of different models that allow considering the joint effect of coastal flooding and erosion in the TWL and coastal flood modelling stages at all, some or none of the scales at which these two impacts interact. Consideration of erosion at any scale involves modelling shoreface changes at such a scale and updating the topobathymetry accordingly, to influence TWL, flooded area or both. In all CAs, surf-zone hydrodynamics and coastal flooding are modelled using XBeach and RFSM-EDA, respectively. The no CA does not consider erosion effects on either TWL computation or flood propagation over land. Conversely, the full CA does account for surf-zone morphodynamics and long-term shoreface translation in TWL computation and for

short- and long-term shoreface changes in the modelling of coastal flooding. Finally, the short- and long-term CA limit erosion consideration to storm morphodynamics in the TWL stage and short-term shoreface erosion in coastal flooding, and to long-term shoreface updates in both TWL and coastal flood modelling stages, respectively. Table 1 summarises the main features of the CA considered, including the time scales of erosion coupling and models used in each case.

2.2. Study area

For illustration purposes, we apply the methodology to a 40-km Spanish Mediterranean coastal stretch located between Castellon and Valencia (Fig. 2). The stretch has a high degree of anthropisation and 10 urban beaches with different configurations that may condition their morphodynamic response and exposure to flooding. Some urban beaches are wide enough that their evolution is not constrained by a non-erodible limit. This is the case for Burriana, where several groynes also help to reduce the effect of the waves on the beach. Unlike Burriana, in Chilches, the evolution of the shoreline and the potential for flooding

Table 1

Summary of main characteristics of the coupling approaches considered in this study. *: when applicable.

Coupling approach (CA)	TWL modelling (XBeach hydrodynamics)		Coastal flood modelling (RFSM-EDA)	
	Long-term erosion	Short-term erosion	Long-term erosion	Short-term erosion
Full CA	ShoreTrans forced with long-term shoreline changes from IH-LANS and SLR*	XBeach Morphodynamics	ShoreTrans forced with long-term shoreline changes from IH-LANS and SLR*	ShoreTrans forced with storm erosion from IH-LANS
Short-term CA	–	XBeach Morphodynamics	–	ShoreTrans forced with storm erosion from IH-LANS
Long-term CA	ShoreTrans forced with long-term shoreline changes from IH-LANS and SLR*	–	ShoreTrans forced with long-term shoreline changes from IH-LANS and SLR*	–
No CA	–	–	–	–

are conditioned by the existence of a promenade. In mixed beaches, such as Almenara and Sagunto, the northern section has a breakwater at the back, and the southern part is more natural and may even maintain the dune system.

These beaches were in dynamic equilibrium due to intense southerly longshore sediment transport offset with continuous sediment uptake until the early 20th century, when the ports of Castellon, Burriana and Sagunto were built. This caused coastline recession on beaches sheltered by structures and advance on down-drifted beaches. Decades later,

massive urban development along a chronically receding coastline exacerbated this imbalance (further details are provided in [Alvarez-Cuesta et al., 2021a; 2021b](#)). Although actions have been taken, the problem persists to this day, and climate change is expected to continue to jeopardise a flat and low coastal stretch where beaches are the primary defence against coastal flooding.

2.3. Climate and exposure data

We use the bias-corrected dynamic multi-model projections of waves and storm surges developed by [IHCantabria \(2020\)](#) for the coast of Spain. RCM atmospheric fields were used as forcing for process-based models to produce hourly time series for the time periods 1986–2005, 2026–2045 and 2081–2100 and for RCP4.5 and RCP8.5. The RCMs used (RCA4 and ALADIN52) and their driving GCMs (IPSL-CM5A-MR, HADGEM2-ES, EC-EARTH, CNRM-CM5 and CNRM-CM5) have time resolutions of 3 and 6 h and spatial resolutions of $0.11^\circ \times 0.11^\circ$ and from 1.25° to 1.90° , respectively. For simplicity, we denote the 5 configurations of GCMs-RCMs as IPSL, HADG, EART, CNRM and MEDC hereinafter. The numerical models used were WaveWatch III ([Tolman, 2014](#)) for waves and ROMS ([Shchepetkin and McWilliams, 2005](#)) for storm surges. We refer the reader to [IHCantabria \(2020\)](#) for more details.

We reconstruct the astronomical tides with the harmonic constituents of the TPXO7.2 global model ([Egbert and Erofeeva, 2002](#)) using Oregon State University Tidal Prediction Software (OTIS) with a horizontal resolution of 0.25° . We extract hourly time series from 1985 to 2100, which in the study area show a mixed diurnal-semidiurnal cycle of approximately 20 cm of tidal range.

SLR is based on SROCC projections ([Oppenheimer et al., 2019](#)). These projections have a resolution of 1° and account for sterodynamic variability, melting of mountain glaciers and ice sheets, land water and glacial isostatic adjustments of 21 GCMs for RCP4.5 and RP8.5. We employ the mean and standard deviation of the multi-model ensemble to compute the likely range (90% confidence band) following the IPCC methodology. As such, we multiply the annual mean by 1.64 times the



Fig. 2. (A) Location of the highly anthropized 40-km coastal stretch between Castellon and Sagunto (Spanish Mediterranean) where the methodology is illustrated. (B) Urban beaches are marked with circles. (C) Examples of different typologies of urban beaches.

annual standard deviation to obtain the 5th and 95th percentiles. On average, the RCP8.5 SLR 5th, 50th and 95th percentiles are expected to reach 0.25, 0.30 and 0.36 m by 2050 and 0.75, 0.89 and 1.01 m by 2100, respectively, along the study coast.

We generate two topobathies by integrating different sources of topographic and bathymetric information. For one topobathy (TB2005), we use the 2009 Digital Terrain Model (DTM) of the Spanish Geographic Institute (IGN) based on LIDAR data with a horizontal resolution of 5 m; the 2009 nearshore bathymetry of Castellon and Valencia of the Spanish Ministry for Ecological Transition and Demographic Challenge (MITECO); and the deep-water bathymetry of the European Marine Observations and Data Network (EMODnet). To obtain the second topobathy (TB2020), we combine the 2016 DTM of the IGN with a horizontal resolution of 5 m (initially 2 m and interpolated to 5 m); an update of the 2009 nearshore bathymetry to 2020 using the PNOA coastline and satellite images (including digitalisation of structures); and EMODnet. In addition, to each cell of the DTMs, we assign a Manning's roughness value inferred from the land uses of the Corinne Land Cover EU database, as done in Toimil et al. (2017a).

2.4. Probabilistic storm modelling

The impact of coastal flooding is usually measured by maximum flood extents and depths due to common TWL events with a likely return period of once every 100 years (e.g., harmonised with the European Flood Directive and other regulations). Obtaining these TWL extreme values, whether from observations or from a single RCM (or GCM) realisation, requires extrapolation of the data, which can result in large confidence limits on estimates (Toimil et al., 2020a). It must be added that the unusual combinations of processes associated with these events make them difficult to forecast because they may be so rare that historical (or simulated) analogues may not have been observed (Milly et al., 2002). Finally, the processes that cause extreme events often interact and are spatially and temporally dependent (Zscheischler et al., 2018). Failure to take this dependence into consideration could lead to misestimation of real risk (Sayol and Marcos, 2018).

In the literature, several studies have proposed multivariate statistical models to increase the population of physically and statistically possible storms (due to waves and storm surges) that could drive coastal flooding (e.g., Wahl et al., 2016; Arns et al., 2017; Sayol and Marcos, 2018; Lucio et al., 2020). These studies stand apart from the widely spread simplifying assumption that the maximum realisations of individual TWL variables or their potential extreme combinations have already been observed or simulated. However, they have the shortcoming that they do not allow the representation of the interdependence relationship between circular variables such as wave direction, and their generalisation to n forcing points and therefore their application on a regional scale is not straightforward.

Here, we generate probabilistic multivariate waves and storm surge extreme events with spatial dependence by setting up a model that couples the monthly-scale extreme multivariate model based on Gaussian copulas presented by Lucio et al. (2020) and the multivariate directional model developed by Mardia et al. (2008a,b) (hereinafter EMM and MDM, respectively), as shown in Eq. (1) by means of the probability density function.

$$f_{Hs_{iw}, Tm_{iw}, Dir_{iw}, SS_{iss}}(Hs_{iw}, Tm_{iw}, Dir_j, SS_{iss}) = \underbrace{f(Hs_{iw}, Tm_{iw}, Dir_j, SS_{iss})}_{EMM} \underbrace{f(Dir_{iw \neq j} | Dir_j)}_{MDM} \quad (1)$$

where H_s is the significant wave height; T_m is the mean wave period; Dir is the wave direction; SS is the storm surge; $iw \in [1, 2, \dots, n]$ are the wave forcing points; n is the total number of emulated points; iss is the storm surge forcing point; and j is the tie point between EMM and MDM. Associated with each deep-water storm, we extract T_p and astronomical tides (AT) by the application of heteroscedastic regression and by

random choice from the harmonic reconstructed time series, respectively, and add the corresponding SLR.

The model represents a generalisation to n forcing points of the conditional relationship between linear and directional variables proposed by Wahl et al. (2016). We couple EMM and MDM by means of a circular link variable j , from which we extract the directions of the rest of the points where the emulator is to be applied ($iw \neq j$), denoted here as director points. Importantly, this approach is valid provided that the link direction captures the dependence between the linear variables and the remaining emulated directions, which allow limiting the conditional dependence modelled with the MDM to a single direction modelled with the EMM. The emulator captures the seasonality of storms by fitting the EMM to the marginal variables monthly.

We apply the multivariate EMM-MDM emulator to derive synthetic storms for each RCP, RCM realisation, and time period (1986–2005, 2026–2045 and 2081–2100) (25 combinations). The first step consists of collecting wave conditions and water levels at locations near the outer contour of what is to be the SWAN propagation grid (boundary points). The second step entails the design and application of a storm selection criterion. We use a TWL indicator that combines AT , SS , wave setup and infragravity swash, the latter two components of which are defined with the semi-empirical formulation of Stockdon et al. (2006) for dissipative beaches:

$$\overline{TWL} = \frac{1}{nt} \sum_{i=1}^{nt} (AT_i + SS_i + (0.016 + 0.03) \sqrt{H_0 L_0}) \quad (2)$$

where nt is the number of forcing points on the contour; and H_0 and L_0 are the wave height and length in deep water, respectively. Note that we neglect the 1.1 skewness factor as we do not consider the high-frequency contribution of waves. This TWL proxy is only used to identify storm conditions from which to extract the forcing variables on which to apply the emulator. Thus, the generated storms are not sensitive to this formulation.

We select monthly maximum \overline{TWL} values from September to April (both included) and their corresponding forcing variables (H_s , T_m , Dir , SS , and AT) for the 25 combinations of RCP, RCM, and time period at all boundary points. This time window allows us to have a population of extreme events large enough to ensure statistical robustness while representing actual storms (in the Mediterranean Sea, storms occur predominantly in late fall, winter, and early spring, as stated in Sayol and Marcos, 2018). After selecting such maximum monthly \overline{TWL} values, we perform a correlation analysis to check the correlation between contour points and identify certain highly correlated groups. We identify the clusters and their centroids (director points) by applying the K-means technique, considering the marine climate of the area and the bathymetry. The next step is the EMM-MDM emulator, which consists of obtaining fitting parameters that can best reproduce the statistical and interdependence relationships of the dynamic simulations of wave conditions and storm surges. We obtain the distribution function of each variable independently and the correlation matrix in the probability space for the EMM and use a mixing distribution composed of several multivariate von Mises distributions (Mardia, 1975; Mardia et al., 2008a,b) for the MDM. The last step is the synthetic generation of monthly extreme events that may cause coastal flooding. We apply Monte-Carlo techniques to emulate 100,000 multivariate storms for all the combinations. We extract random realisations of the EMM (Hs_{iw} , Tm_{iw} , Dir_j and SS_{iss}) that couple with the MDM through Dir_j , which also allows the remaining Dir_{iw} to be randomly determined.

2.5. Long- and short-term topo-bathymetry updates

The objective of topobathy updates is to account for long-term shoreface changes in surf-zone hydrodynamic modelling (including morphodynamics) and long-term shoreface changes and storm erosion

in hydraulic modelling. When coastal flooding and erosion are fully coupled, we first perform the long-term topobathy translation (diagonal or forward-backward profile displacement depending on the type of sediment transport), then the hydrodynamic modelling and finally the short-term topobathy adjustment (storm-driven erosion of the upper part of the profile and deposition in the lower part). In the simplified approaches, only one topobathy update applies in each case.

For the topobathy update, we first develop a two-level shoreline discretisation, from which we obtain one set of low-resolution (LR) transects (spaced 200 m apart) and one set of high-resolution (HR) transects (spaced 10 m apart). The LR set is used as a guardrail to guide shoreline change estimates (forward or backwards movement) obtained with IH-LANS, a multi-process numerical model that has shown skill in predicting shoreline evolution in highly anthropised coasts (Alvarez-Cuesta et al., 2021a). IH-LANS has a hybrid nearshore downscaling tool that allows the incorporation of detailed wave spectral information (spectral partitions) from RCMs and a breaking propagation routine. In response to waves and water levels, the model computes longshore and cross-shore transport considering the effects of human interventions (Eq. (3)). IH-LANS yields a time series of shoreline positions with reduced calibration uncertainty, as it integrates an extended Kalman filter for the assimilation of shoreline observations.

$$\begin{aligned} \underbrace{\frac{\partial Y}{\partial t}}_{\text{Total shoreline change}} &= \underbrace{\frac{\partial Y_l}{\partial t}}_{\text{Longshore shoreline changes}} + \underbrace{\frac{\partial Y_c}{\partial t}}_{\text{Cross-shore shoreline changes}} \\ \frac{\partial Y_l}{\partial t} &= \underbrace{-\frac{1}{B+d_c} \frac{\partial Q}{\partial x}}_{\text{Longshore transport gradients}} + \underbrace{\frac{1}{B+d_c} q}_{\text{Sediment sinks and sources}} + \underbrace{vlt}_{\text{unresolved processes}} \\ \frac{\partial Y_c}{\partial t} &= K_c^{+/-} [Y_c^{\text{eq}} - Y_c] \end{aligned} \quad (3)$$

where Y is the distance measured along the transect from a reference line (e.g. the onshore profile point) to the shoreline (mean high-water contour) and computed as the summation of the shoreline position associated with longshore (Y_l) and cross-shore processes (Y_c). B is the berm height; d_c is the depth of closure; $\partial Q/\partial x$ are the longshore transport gradients; q/d_c is the shoreline change rate due to sediment sinks ($q < 0$) and sources ($q > 0$); vlt is a long-term trend that accounts for unresolved processes (assimilation residue); $K_c^{+/-}$ is the cross-shore accretion/erosion rate; and Y_c^{eq} defines the cross-shore equilibrium position. In IH-LANS, the longshore transport gradients are computed using the CERC equation (USACE, 1984), which depends on the energy flux in the breaker zone.

The cross-shore equilibrium position (Y_c^{eq}) is defined following Miller and Dean (2004) but including the tide effects, as in Toimil et al. (2017b):

$$Y_c^{\text{eq}} = \Delta y_0 - W_b \left(\frac{0.106 H_b + SS + AT}{B + h_b} \right) \quad (4)$$

where Δy_0 is an empirical constant that assures that short-term fluctuations oscillate around a baseline position, W_b is the surf zone width calculated assuming a Dean's shaped profile (Dean, 1991) $W_b = (H_b/\gamma A)^{1.5}$, H_b is the breaking wave height, γ is the wave breaking coefficient ($\gamma = 0.55$), A is the Dean's profile parameter and h_b is the depth of breaking $h_b = H_b/\gamma$.

The extended Kalman filter allows IH-LANS to assimilate observations and self-calibrate its free parameters, which are the longshore transport constant of the CERC equation, the cross-shore accretion and erosion rates ($K_c^{+/-}$) and the unresolved processes trend (vlt).

According to Eq. (3), the shoreline response to wave and sea level conditions has a longshore and a cross-shore component, which are modelled uncoupled and then added. Longshore transport gradients and SLR effects (in this case not considered with IH-LANS but with ShoreTrans) are long-term processes (i.e., from years to decades) that result from mean climate conditions. Short-term cross-shore sediment transport occurs at shorter time scales and includes seasonal and interannual shoreline variations and storm erosion due to extreme weather events.

We use long- and short-term estimates of shoreline change from IH-LANS simulations together with SLR to force ShoreTrans along the 4137 HR transects. ShoreTrans is a simple, rule-based, user-input-driven, shoreface translation and sediment budgeting model that applies surveyed profiles to estimate changes in realistic coastlines that result from SLR and variations in sediment supply (McCarroll et al., 2021). The main difference between ShoreTrans and other methods for translating surveyed profiles is that ShoreTrans explicitly resolves volume conservation over real profiles rather than theoretical ones (e.g., in Erikson et al., 2017, a Bruun-like profile is used to determine the landwards and upwards movement of the surveyed profiles due to SLR).

ShoreTrans uses different algorithms to update profiles depending on the time scale of the processes considered. Profile parameterisation and kinematics are shown in Fig. 3. For long-term processes (long-shore transport and SLR), the active depth extends between the berm (y_b, z_b) and the depth of closure (y_{dc}, z_{dc}). For short-term erosion, profile reference points are beachface top (y_{tb}, z_{tb}), the beachface bottom (y_{bb}, z_{bb}), the erosion-accretion inflection point (y_p, z_p) and the storm bar bottom (y_{sb}, z_{sb}). Longshore transport kinematics alter the initial profile by a shoreward (erosion) or seaward (accretion) movement (Fig. 3b). In case of short-term erosion, the beachface recedes inland and an erosion wedge is formed until the pivot point (Fig. 3c). This process is assumed to produce a net zero volume change. As a result, an accreted sinusoidal shape is generated between the pivot point and the storm bar bottom. The mechanism of the translation model due to SLR is to shift the active profile up by the change in sea level and onshore to the point at which net volume change is zero (diagonal profile shift, Fig. 3d). In case of a Dean's shaped profile (Dean, 1991), the shoreward movement coincides with the Bruun's rule retreat (Bruun, 1962). As such, while long-term processes are modelled through a simple active profile translation, profile displacement associated with short-term erosion implies beachface changes and the formation of an erosion bar.

2.5.1. Long-term topo-bathymetry update

We compute an indicator of long-term shoreline change (progradation or retreat) along each LR transect for 2045 and 2100 relative to 2020 (hereinafter C2045 and C2100, respectively) by subtracting the 2-year average initial position ($Y_{l,t}$) from the 2-year average final posi-

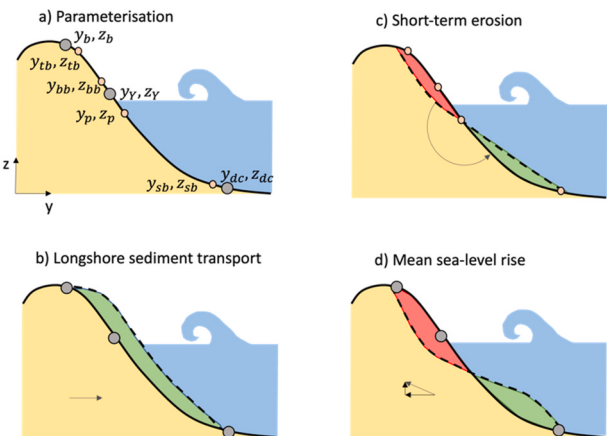


Fig. 3. Parameterisation and representation of profile kinematics used in ShoreTrans.

tion of the shoreline ($Y_{l,t+1}$) from each IH-LANS RCP-RCM simulation. We assign LR transect-related C2045 and C2100 values to HR transects using distance-based interpolation. We transform these shoreline shifts into HR profile volumes (hereinafter V2045 and V2100, in m^3/m) by multiplying them by the RCP-RCM active depth computed at each HR transect in 2045 and 2100 following:

$$\Delta V = (Y_{l,t+1} - Y_{l,t})(B + d_c) \quad (5)$$

where Y_l refers to the longshore shoreline position calculated using the first right-hand side term in Eq. (3).

Given an initial profile defined by its in-plane $y(t)$ and $z(t)$ coordinates, the new elevation at time ($t + 1$) results:

$$z_{t+1}(y) = z_t(y - \Delta Y) + \Delta SLR \quad a < y < b \quad (6)$$

where ΔY is the unknown horizontal displacement associated with both longshore and SLR changes; and ΔSLR is the vertical profile displacement between instant t and $t+1$. The domain is bounded by the active profile, being at the onshore limit $a = y_b + \Delta Y$ and b the offshore limit $b = y_{dc} + \Delta Y$.

To solve for ΔY , $F(\Delta Y)$ is solved algorithmically with an optimisation routine that minimises it.

$$F(\Delta Y) = \int_a^b [z_{t+1}(y) - z_t(y)] dy + \Delta V \quad (7)$$

where V is the net profile volume change due to longshore processes (V2045 and V2100) from IH-LANS (Eq. (5)).

This approach considers three cases: $\Delta SLR = 0$; $\Delta V \neq 0$ no change due to SLR and longshore volume change in the profile (Fig. 3b); $\Delta SLR \neq 0$; $\Delta V = 0$ change due to SLR without longshore volume change in the profile (Fig. 3d); and $\Delta SLR \neq 0$; $\Delta V \neq 0$ change due to SLR and longshore volume change in the profile (Fig. 3b and d).

In the case of a seawall, we apply the same procedure and then transfer the potential erosion in the shoreward part of the non-erodible structure to the offshore area adjacent to the wall. The eroded sediment is distributed in a triangular wedge that extends offshore a distance equal to 1/3 of the extent of the active profile from the structure's toe.

We apply ShoreTrans for 3 sets of forcing conditions: 1) RCP-averaged V2045 and SLR 50th percentile in 2045; 2) RCP4.5 V2100 and SLR 50th percentile in 2100; and 3) RCP8.5 V2100 and SLR 50th percentile in 2100. Using TB2020 as the baseline we obtain 3 new sets of HR transects: 1 for 2045 (RCP averaged) and 2 for 2100 (for RCP4.5 and RCP8.5). We transform each set of HR transects into a grid of points (1×10 m) that we interpolate to generate TB2045LT, TB2100LT_RCP4.5 and TB2100LT_RCP8.5, all with a resolution of 5x5 m. The area not covered by the profile interpolation (i.e., that beyond beaches) is filled with TB2020 (5 × 5 m).

2.5.2. Short-term topo-bathymetry update

We force the 2D flood model with return periods of TWL obtained from fitting an extreme value function to a sample of thousands of storms, some of which are modelled using SWAN (offshore to nearshore propagation) and XBeach (hydrodynamics and morphodynamics computation) and the rest reconstructed using statistical tools. Morphodynamic changes associated with TWL return periods are thus unknown. Without such information available, we compute an average storm erosion from IH-LANS simulations and use it as input for ShoreTrans to produce ST and FULL topobathies over TB2020 and LT topobathies, respectively.

We determine the magnitude of large yet representative storm erosion events along LR transects by identifying erosion peaks above the 95% threshold (Fang et al., 2013) from each RCP-RCM cross-shore shoreline position simulation (second right-hand side term in Eq. (3)) and averaging their values over 1986–2005, 2026–2045 (RCP averaged) and 2081–2100 (for RCP4.5 and RCP8.5). As such, we obtain only one

average storm representative of the conditions associated with each topobathy. We interpolate LR cross-shore shoreline retreat to HR transects using distance-based interpolation and transform them into storm profiles following the approach of Kinsela et al. (2017), included in ShoreTrans. This approach considers the storm-response kinematics represented in Fig. 3c.

We translate each set of HR transects into a grid of points (1×10 m) that we interpolate to generate TB2005ST/TB2005FULL, TB2045ST, TB2100ST_RCP4.5 and TB2100ST_RCP8.5 (on TB2005 the first and TB2020 the rest) and TB2045FULL, TB2100FULL_RCP4.5 and TB2100FULL_RCP8.5 (on TB2045LT, TB2100LT_RCP4.5 and TB2100LT_RCP8.5, respectively), all with a resolution of 5x5 m. The area not covered by the profile interpolation is filled with the corresponding reference topobathy (5×5 m).

For clarity, Table 2 summarises the topobathies generated in this study, including the basis on which they are made and the processes incorporated in ShoreTrans for their production.

2.6. Hybrid downscaling and hydro-morphodynamic modelling

We consider that the wave contribution to TWL occurs in terms of dynamic wave setup (DWS). DWS can be defined as the sustained elevation of the water level due to the transference of wave-related momentum to the surf zone (static setup) plus a long-period oscillating component. Although DWS can be determined semi-empirically (Gomes da Silva et al., 2020), the complex interactions that occur between hydrodynamics and morphodynamics can be accounted for only by means of numerical modelling.

Here, we apply a hybrid downscaling methodology (following that of Camus et al., 2011) that combines statistical tools (a selection algorithm and RBFs) and numerical models (SWAN, Booij et al., 1999; and XBeach 1D) to compute the DWS and associated morphological changes. The first step is the definition of the computational domain for SWAN, which is composed of one global grid (500×500 m) one-way nested to three high-resolution grids (50×50 m). The global grid must be aligned with the storm modelling, as the wave conditions and water levels required to generate the storms have to be collected at the outer contour points of this grid. In the second step, we apply the maximum dissimilarity algorithm to select 5 subsets of storms with 500 cases each that well represent the full sample of storms for each topobathy. The third step is the propagation of the selected storm-related wave conditions using SWAN. We obtain 4x500 cases of wave parameters at a 10 m depth every 200 m along the coast.

The next step is the extraction of 5 sets of 247 beach profiles (coincident in space with LR transects, spaced 200 m apart) from the topobathy TB2005 (reference) and from topobathies TB2020, TB2045,

Table 2
Summary of main characteristics of the topobathies generated in this study.

Topo-bathymetry	Baseline topo-bathymetry	ShoreTrans processes
TB2005	IGN (2009) + MITECO (2009)	–
TB2005ST	TB2005	Short-term erosion
TB2020	IGN (2016) + MITECO (2020)	–
TB2020ST	TB2020	Short-term erosion
TB2045ST	TB2020	Short-term erosion
TB2045LT	TB2020	Long-term shoreline changes & SLR
TB2045FULL	TB2045LT	Short-term erosion
TB2100ST_RCP4.5	TB2020	Short-term erosion
TB2100LT_RCP4.5	TB2020	Long-term shoreline changes & SLR
TB2100FULL_RCP4.5	TB2100LT_RCP4.5	Short-term erosion
TB2100ST_RCP8.5	TB2020	Short-term erosion
TB2100LT_RCP8.5	TB2020	Long-term shoreline changes & SLR
TB2100FULL_RCP8.5	TB2100LT_RCP8.5	Short-term erosion

TB2100_RCP4.5 and TB2100_RCP8.5. Profiles extend from a depth of 10 m to the berm, taking advantage of the nearshore downscaled storm-related wave conditions. We run calibrated XBeach (see Supplementary Material for details) over these profiles to solve DWS and morphodynamics related to the corresponding subsets of 500 storms. We force XBeach with a series of hourly JONSWAP spectra that generate a 72-h synthetic storm (a typical value of storm duration accepted for the Mediterranean Sea region, Marcos et al., 2009). The shape of the storm is parametrized based on historic records and accounts for water levels (SS, AT and SLR). The last step is the reconstruction of the complete sample of DWS using RBFs. RBFs allow us to define statistical relationships between offshore wave parameters and surf-zone conditions, which are the outputs of XBeach.

2.7. Extreme value analysis and hydraulic modelling

Once the hybrid method is completed, we compute TWLs associated with the 100,000 storms for the 25 combinations of RCP, RCM, and time period by summing DWSs and their corresponding SSs and ATs linearly. We fit a 3-parameter generalised extreme value (GEV) distribution to each of the 25 sets of 100,000 values. Although future storms account for climate change in the distribution of wave conditions and storm surges over time, intra-period variation trends are not significant, so a stationary fit can be justified in this case (see Supplementary Material for further details).

Table 3

TWL modelling characteristics for the scenarios considered. ShoreTrans and XBeach inputs and forcing conditions. *: We simulate 500 storms representative of the conditions associated with each topobathy and then use these simulations to reconstruct the complete sample.

Scenario & CA	TWL modelling characteristics				
	Baseline topo-bathymetry	ShoreTrans forcing conditions	XBeach topo-bathymetry	XBeach modules activated	XBeach forcing conditions
2005 NO/LT CA	TB2005	–	TB2005	Hydrodynamics	100,000* storms for each RCM over 1985–2005 (cluster 1)
2005 ST/FULL CA	TB2005	–	TB2005	Hydrodynamics & morphodynamics	
2045 NO CA	TB2020	–	TB2020	Hydrodynamics	100,000* storms for each RCP-RCM combination over 2026–2045 and 2081–2100 (cluster 2) & 3 SLR percentiles
2045 ST CA	TB2020	–	TB2020	Hydrodynamics & morphodynamics	
2045 LT CA	TB2020	RCP-averaged V2045 from IH-LANS and SLR 50th percentile in 2045	TB2045LT	Hydrodynamics	100,000* storms for each RCP-RCM combination over 2026–2045 (cluster 3) & 3 SLR percentiles
2045 FULL CA	TB2045LT	–	TB2045LT	Hydrodynamics & morphodynamics	
2100 RCP4.5 NO CA	TB2020	–	TB2020	Hydrodynamics	100,000* storms for each RCP-RCM combination over 2026–2045 and 2081–2100 (cluster 2) & 3 SLR percentiles
2100 RCP4.5 ST CA	TB2020	–	TB2020	Hydrodynamics & morphodynamics	
2100 RCP4.5 LT CA	TB2020	RCP4.5 V2100 from IH-LANS and SLR 50th percentile in 2100	TB2100LT_RCP4.5	Hydrodynamics	100,000* storms for each RCP4.5-RCM combination over 2081–2100 (cluster 4) & 3 RCP4.5 SLR percentiles
2100 RCP4.5 FULL CA	TB2100LT_RCP4.5	–	TB2100LT_RCP4.5	Hydrodynamics & morphodynamics	
2100 RCP8.5 NO CA	TB2020	–	TB2020	Hydrodynamics	100,000* storms for each RCP-RCM combination over 2026–2045 and 2081–2100 (cluster 2) & 3 SLR percentiles
2100 RCP8.5 ST CA	TB2020	–	TB2020	Hydrodynamics & morphodynamics	
2100 RCP8.5 LT CA	TB2020	RCP8.5 V2100 from IH-LANS and SLR 50th percentile in 2100	TB2100LT_RCP8.5	Hydrodynamics	100,000* storms for each RCP8.5-RCM combination over 2081–2100 (cluster 5) & 3 RCP8.5 SLR percentiles
2100 RCP8.5 FULL CA	TB2100LT_RCP8.5	–	TB2100LT_RCP8.5	Hydrodynamics & morphodynamics	

Having such a large population of storms allows us to determine TWL values of high return periods that are statistically robust because they are based on the EMM-MDM emulator. We obtain the 100-year TWL (TWL₁₀₀) in the time horizons (H) 2045 and 2100 (plus the baseline 2005), to which we add SLR (5th, 50th and 95th percentiles) for the different RCPs. These TWL₁₀₀ values are used to define tidal profiles with a shape similar to that of the Storm Gloria peak, which are the forcings of the 2D flood model that we use to produce flood maps.

RFSM-EDA (Jamieson et al., 2012) is an efficient hydraulic model that provides water depth over ground following the impact-zone approach (Gouldby et al., 2008) but incorporates the local acceleration term of the Saint Venant equations and an adaptive time step. Its algorithm allows the consideration of topography as a sub-element in a computational mesh that adapts to the terrain features, and it is sensitive to Manning's roughness.

3. Results

The most important outcomes of the methodology are the generation of multivariate projected storms (that we then propagate from deep water to the surf zone); the updating of the topobathies on which we simulate TWL and/or coastal flooding based on SLR and projections of long-term shoreline changes and storm erosion; and the analysis of the influence of the combined effect of future storms and shoreface changes on the TWL and the flooded area. For the scenarios and CA considered,

Table 3 and **Table 4** summarises the main characteristics of the TWL and coastal flood modelling, including ShoreTrans, XBeach and RFSM-EDA inputs and forcing conditions. We elaborate on the results and analyse the contribution of each climate-related uncertainty source to the TWL and the flooded area.

3.1. Probabilistic storm conditions

We apply an EMM-MDM emulator composed of two coupled multivariate models (extreme-based and directional) to generate multivariate storms at the regional scale considering spatial dependence. While the EMM allows us to capture the dependence between linear variables, for circular variables, we apply the MDM. For instance, **Fig. 4** shows the probability density function of the MDM for RCP4.5 MEDC 2026–2045, where three mono-modal multivariate von Mises $T_{\theta}(\theta)$ distributions are fitted to three clusters. We combine these distributions with their occurrence probabilities to obtain the mixing multivariate directional distribution $f_{\theta}(\theta)$ that considers all possible incoming storm directions, where the most likely cluster (probability of 0.64) has a mode centred on $\text{Dir}_3 = 63^\circ$, $\text{Dir}_6 = 65^\circ$ and $\text{Dir}_9 = 70^\circ$. We fit the EMM to three director points and derive the monthly cross-correlation matrix of the variables involved (H_{S3} , H_{S6} , H_{S9} , T_{m3} , T_{m6} , T_{m9} , Dir_6 , and SS_5), which are transformed to the probability space through their marginal distribution functions. We select the directional clusters of the MDM and the director points of the EMM based on bathymetric changes and the marine climate of the area, respectively.

We generate 100,000 multivariate storms for the 25 combinations of RCP, RCM, and time period. The emulator can capture the physics of

wave generation with respect to the interdependence between the variables. As an example, **Fig. 5** shows the skill of the EMM-MDM in reproducing the statistical relationships between the linear variables H_{S3} , T_{m3} and SS_5 and the circular variable Dir_3 by the conditional dependence through Dir_6 . We represent both the observations and statistical emulation in matrix form. Panels a–f illustrate the scatter plots of observed and simulated data; Panels e–j show the univariate GEV annual distribution function of H_{S3} , T_{m3} and SS_5 and the empirical polar density function of Dir_3 ; and Panels k–p represent the comparison between the observed and emulated empirical bivariate density functions, where the goodness of fit of the MME is quantitatively validated. Additional information and validation figures can be found in the Supplementary Material.

For the synthetic generation of storms, we enter the marginal distribution of each variable with normal random vectors and then extract k random realisations of the vector $[H_{S3}, H_{S6}, H_{S9}, T_{m3}, T_{m6}, T_{m9}, \text{Dir}_6, SS_5]_k$. All the EMM realisations are linked to the MDM through Dir_6 . In every case, Dir_3 and Dir_9 are obtained from the MDM by randomly extracting a realisation of the conditional density trivariate function $f_{\text{Dir}_3, \text{Dir}_9 | \text{Dir}_6}(\text{Dir}_3, \text{Dir}_9 | \text{Dir}_6)$. T_p is determined from the calibrated heteroscedastic model, and AT values are derived by selecting a random value of the month and year from the time series of AT reconstructed from harmonics.

3.2. Long- and short-term topo-bathymetry updates

We use the IH-LANS simulations produced by Alvarez-Cuesta et al. (2021b), which consist of an hourly time series of shoreline changes

Table 4
Coastal flood modelling characteristics for the scenarios considered. ShoreTrans and RFSM-EDA inputs and forcing conditions.

Scenario & CA	Coastal flood modelling characteristics			
	Baseline topo-bathymetry	ShoreTrans forcing conditions	RFSM-EDA topo-bathymetry	RFSM-EDA forcing conditions
2005 NO/LT CA	TB2005	–	TB2005	TWL ₁₀₀ for each RCM
2005 ST/FULL CA	TB2005	Average storm erosion over 1986–2005 from IH-LANS	TB2005ST/FULL	
2045 NO CA	TB2020	–	TB2020	TWL ₁₀₀ for each RCP-RCM combination & 3 SLR percentiles
2045 ST CA	TB2020	RCP-averaged average storm erosion over 2026–2045 from IH-LANS	TB2045ST	
2045 LT CA	TB2020	RCP-averaged V2045 from IH-LANS & SLR 50th percentile in 2045	TB2045LT	
2045 FULL CA	TB2045LT	RCP-averaged average storm erosion over 2026–2045 from IH-LANS	TB2045FULL	
2100 RCP4.5 NO CA	TB2020	–	TB2020	TWL ₁₀₀ for each RCP4.5-RCM combination & 3 RCP4.5 SLR percentiles
2100 RCP4.5 ST CA	TB2020	RCP4.5 average storm erosion over 2081–2100 from IH-LANS	TB2100ST_RCP4.5	
2100 RCP4.5 LT CA	TB2020	RCP4.5 V2100 from IH-LANS and SLR 50th percentile in 2100	TB2100LT_RCP4.5	
2100 RCP4.5 FULL CA	TB2100LT_RCP4.5	RCP4.5 average storm erosion over 2081–2100 from IH-LANS	TB2100FULL_RCP4.5	
2100 RCP8.5 NO CA	TB2020	–	TB2020	TWL ₁₀₀ for each RCP8.5-RCM combination & 3 RCP8.5 SLR percentiles
2100 RCP8.5 ST CA	TB2020	RCP8.5 average storm erosion over 2081–2100 from IH-LANS	TB2100ST_RCP8.5	
2100 RCP8.5 LT CA	TB2020	RCP8.5 V2100 from IH-LANS and SLR 50th percentile in 2100	TB2100LT_RCP8.5	
2100 RCP8.5 FULL CA	TB2100LT_RCP8.5	RCP8.5 average storm erosion over 2081–2100 from IH-LANS	TB2100FULL_RCP8.5	

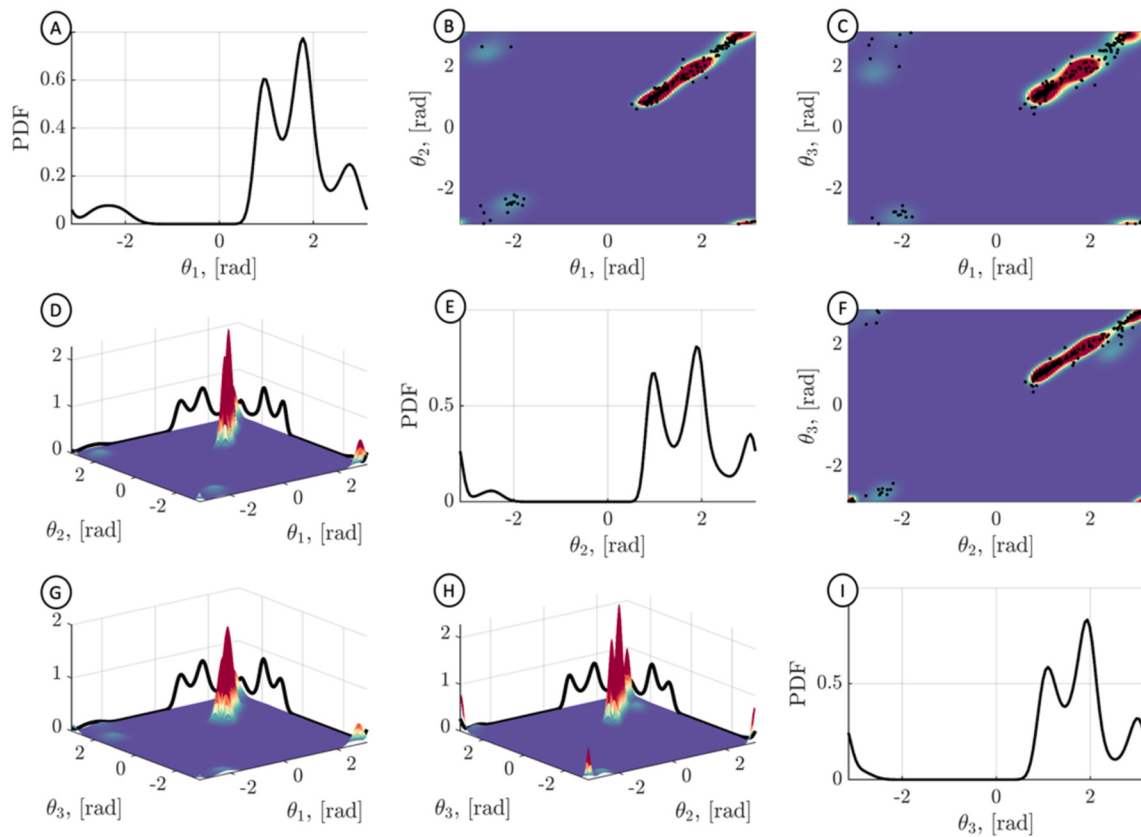


Fig. 4. Probability density function of the MDM for the RCP4.5-MEDC-2026-2045 combination. Panels b, c and f represent the discrete observations over the fitted probability density function. Panels a, e and i show the multi-modal marginal distributions. Panels d, g and h show the bivariate representation of the trivariate density function and their marginal distributions in space.

from 1990 to 2100. By means of an extended Kalman filter, free-model parameters were self-calibrated and validated over the periods 1990–2010 and 2010–2020, respectively, using satellite-derived observations, thus allowing us to reduce knowledge uncertainty. Satellite-derived shorelines were obtained from the Landsat-5, Landsat-8 and Sentinel-2 campaigns using the Coast-Sat algorithm (Vos et al., 2019). To produce these simulations, IH-LANS was forced with wave and storm surge projections for 2 RCPs and 5 RCMs (IHCantabria, 2020) and the reconstruction of the astronomical tide. We obtain the shoreline positions in 2045 and 2100 by joining the HR transect-related RCP-averaged C2045, RCP4.5 C2100 and RCP8.5 C2100 along the coast of study. The contribution of longshore sediment transport to long-term coastline position is substantial on some beaches, leading to erosion and accretion at approximately 30 m (in 40% of the beaches) and 15 m (in 30% of the beaches) in 2050 and up to 90 m and 35 m in 2100, respectively. Although we find that the results are very similar between RCPs, considering that SLR is an additional input for ShoreTrans, we average shoreline changes in 2045 but not in 2100.

We apply ShoreTrans and obtain 4137 HR transects updated in response to the combined effect of longshore sediment transport (RCP-averaged V2045, RCP4.5 V2100 and RCP8.5 V2100 from IH-LANS) and SLR (RCP-averaged 2045, 2100 RCP4.5 and 2100 RCP8.5 50th percentile). Surveyed beach profiles are translated landwards/seawards due to longshore transport and upwards and landwards while conserving volume due to SLR. Comparing long-term updated topobathies with TB2020 allows us to assess the volume of sediment accreted or eroded, the volume of sediment mobilised, and the sediment budget (gains/losses). As an example, Fig. 6 shows long-term erosion and accretion patterns for TB2045LT, TB2100LT_RCP4.5 and TB2100LT_RCP8.5 with respect to TB2020 in Nules and Corinto. In Nules, beach compartments between groynes rotate counter-clockwise

following the direction of the mean wave energy flux (northeast), which is further accentuated in 2100 at the same time as they retreat, especially for the RCP8.5. Due to SLR and longshore transport, the sediment volume mobilised in Nules in 2045 increases at the end of the century by 97% for RCP4.5 and beyond 100% for RCP8.5.

In Corinto, sediment gains in 2045 almost triple those in 2100 regardless of the RCP. Corinto is second to Canet, the beach where the most sediment is mobilised in any event (175,523.69 m³ in 2045 and up to 451,758.71 m³ in 2100), having both erosion and accretion volumes increased with time and radiative forcing. Overall, longshore drift causes the northern beaches (Torre, Burriana, Nules, Moncofar, Chilches, Llosa and Almenara) to lose sediment, which accumulates in the southern beaches (Corinto, Canet and Sagunto).

Additionally, Fig. 6 shows SLR-driven erosion and deposition patterns in the Nules and Corinto surveyed profiles. Using the time series of shoreline evolution from IH-LANS (Alvarez-Cuesta et al., 2021b), we also obtain average storm erosion along each HR transect for 1986–2005, (RCP-averaged) 2026–2045, and (RCP4.5 and RCP8.5) 2081–2100 considering each RCP-RCM simulation. The results show that the beaches with the highest average storm erosion are Canet (13.92–16.12 m), Corinto (13.17–15.16 m) and Sagunto (10.80–12.50 m), a ranking that is maintained for the different periods and RCPs. Fig. 7 presents storm erosion and accretion patterns in Llosa for TB2005FULL with respect to TB2005 and for TB2045FULL, TB2100FULL_RCP4.5 and TB2100FULL_RCP8.5 with respect to TB2045LT, TB2100LT_RCP4.5 and TB2100LT_RCP8.5, respectively. As can be observed, unlike long-term shoreface translation, storm erosion results in a readjustment of sand volumes that erode at the beach front and are deposited in the lower part of the surveyed profiles, making them more dissipative. As we move farther away in time and for higher radiative forcing, the long-term topobathy is set back further, and above

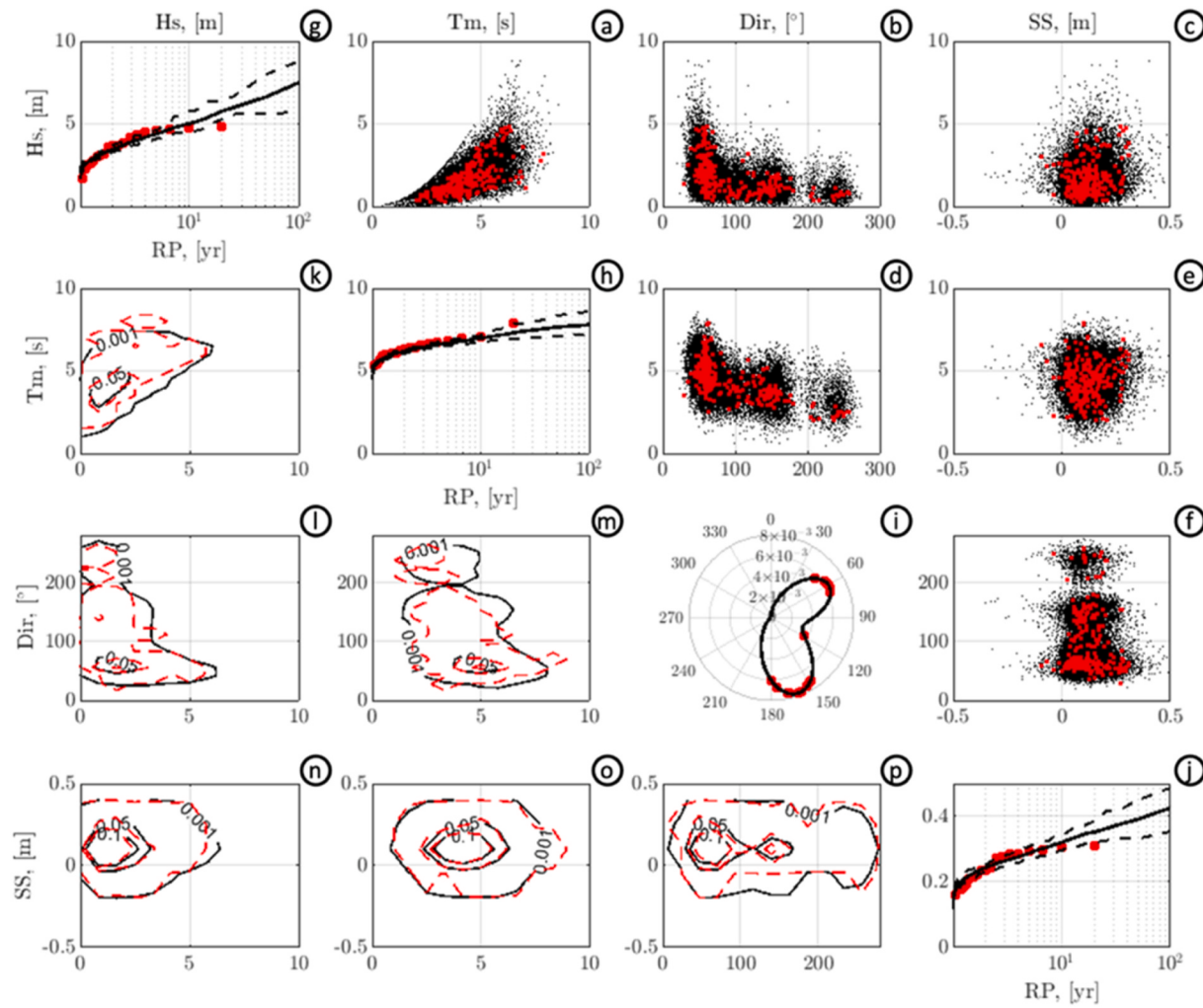


Fig. 5. Validation of the EMM-MDM emulator in one of the director points (point 3). Observations (red) are compared to simulated data (black).

that, storm erosion pushes the coastline further backwards (with blue and green solid lines corresponding to long-term and full CAs, respectively). The storm volumes displaced in Llosa amount to 23523.10 m³ (2005), 22641.96 m³ (RCP-averaged 2050), 24698.41 m³ (RCP4.5 2100) and 19478.12 m³ (RCP8.5 2100).

3.3. Effect of the coupling approach on total water level estimates

To analyse the effect of considering shoreface changes on TWL, we compare the results of the 4 CAs. As shown in Table 2, for the reference period, we simulate all the CAs over TB2005, where the full and short-term CAs and the long-term and no CAs are coincident due to the non-consideration of SLR and because TB2005 is based on 2009 LIDAR data, respectively. For future TWL simulations, we consider TB2020 for the short-term and no CAs, as no long-term shoreface translation applies, and TB2045LT, TB2100LT_RCP4.5 and TB2100LT_RCP8.5 for the full and long-term CAs (Table 3). In full and short-term CA simulations, XBeach morphodynamics is enabled (Table 1).

Fig. 8 presents the probability density functions (PDFs) of TWL in Almenara for the full CA. The first row of panels shows the 5 GEV fits (each of which is based on 100,000 TWL values) for each RCM and RCP (when applicable) in 2005, 2045 and 2100. Future fits are shifted upwards based on SLR percentiles. The second and third panel rows allow visualisation of two examples: RCM variability for the SLR 50th percentile and SLR variability for the EART model, respectively. Looking at the SLR variability, the TWL₁₀₀ spread range becomes larger for

longer time horizons and higher radiative forcing. If focusing on the SLR 50th percentile, the inter-RCM TWL₁₀₀ spread range moves upwards in 2045 (up to 1.80–2.20 m) and 2100 (up to 1.95–2.35 m) with respect to 2005 (~1.70–1.95 m). For the EART model, the variation in the spread range between RCPs is smaller in 2045 than in 2100. This is affected by the divergence of RCP-SLR in 2100 and by the shape of the beach profile, as changes in the foreshore slope in the profile section where sea level oscillates modulate the wave setup and hence the TWL spread range. Shoreface changes also play a key role in TWL inter-CA variability. If the long-term CA were applied, in 2005, 2045 and 2100 (RCP4.5), extreme TWL estimates would be close to those of no CA, as in Almenara, storms smoothen the foreshore slope more than SLR. In 2100 (RCP8.5), a higher SLR would cause these effects to offset each other, with short- and long-term CAs yielding similar values. The standard approach (no CA) could lead to overestimation of TWL₁₀₀ by up to 25% (~5% mean values) with respect to the full CA. The equivalent PDFs of TWL for the short-term, long-term and no CAs are shown in the Supplementary Material. Although longshore transport seems to have no influence on TWL (as it does not modify the shape of the shoreface), this may not necessarily be the case in situations of coastal squeeze when the coastline reaches its non-erodible limit (e.g., a seawall or a promenade).

To further analyse the influence of the choice of the CA on TWLs, Fig. 9 shows TWL₁₀₀ values factorised by CA and grouped by time horizon and RCP in Burriana, Chilches, Almenara, and Sagunto. As SLR progresses, the full and short-term CAs diverge. Almenara and Chilches follow the same pattern, as do Burriana and Sagunto, which relates to

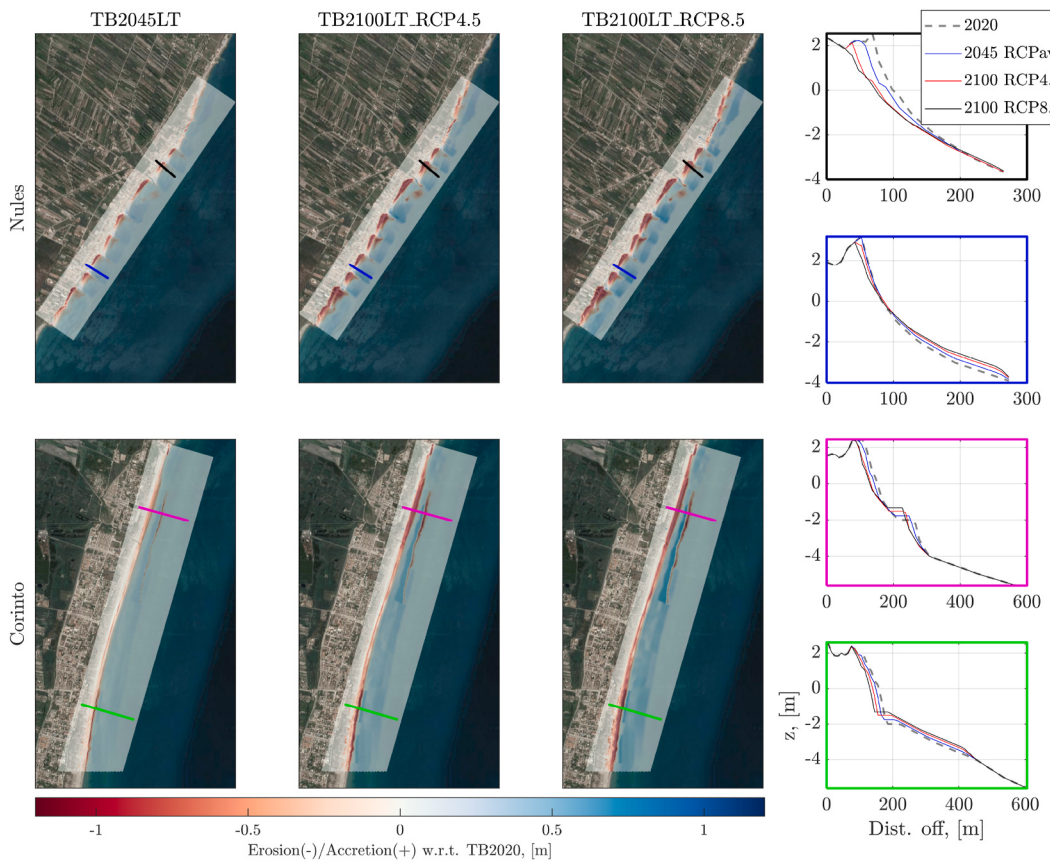


Fig. 6. Long-term erosion and accretion patterns in Nules and Corinto for TB2045LT, TB2100LT_RCP4.5 and TB2100LT_RCP8.5 with respect to TB2020.

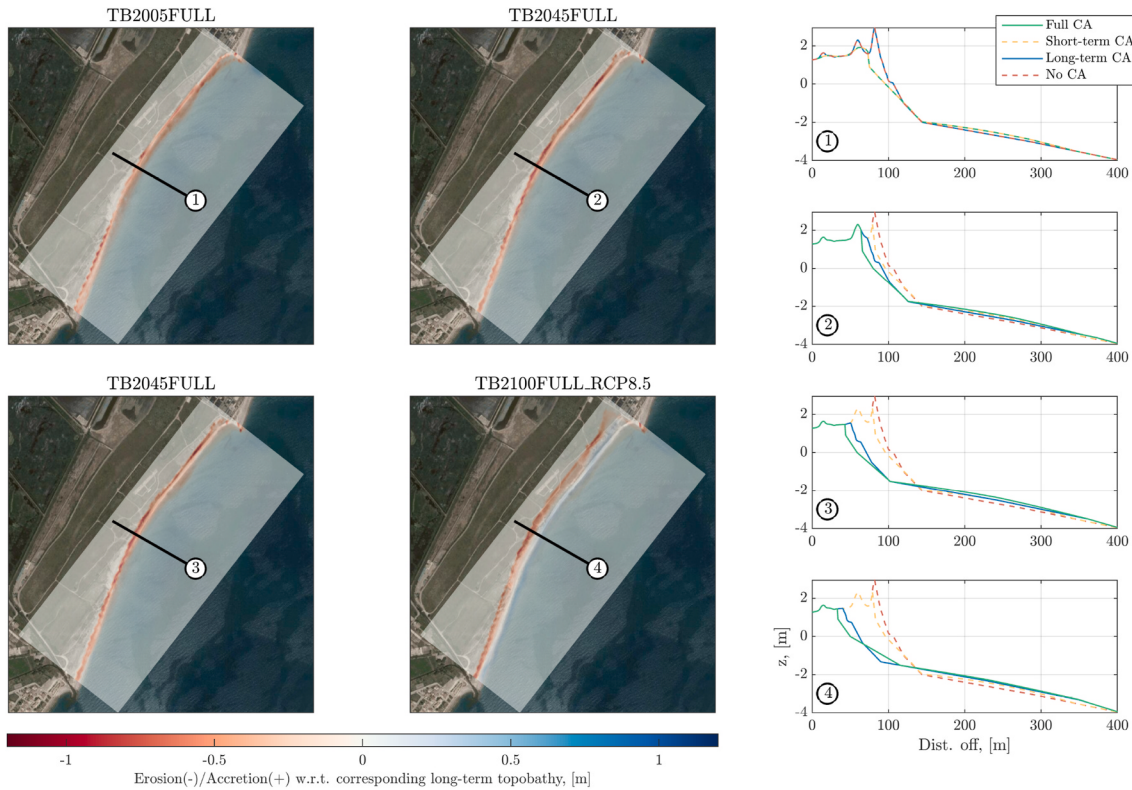


Fig. 7. Short-term erosion and accretion patterns in Llosa for TB2005FULL with respect to TB2005 and for TB2045FULL, TB2100FULL_RCP8.5 and TB2100FULL_RCP8.5 with respect to TB2045LT, TB2100LT_RCP4.5 and TB2100LT_RCP8.5, respectively.

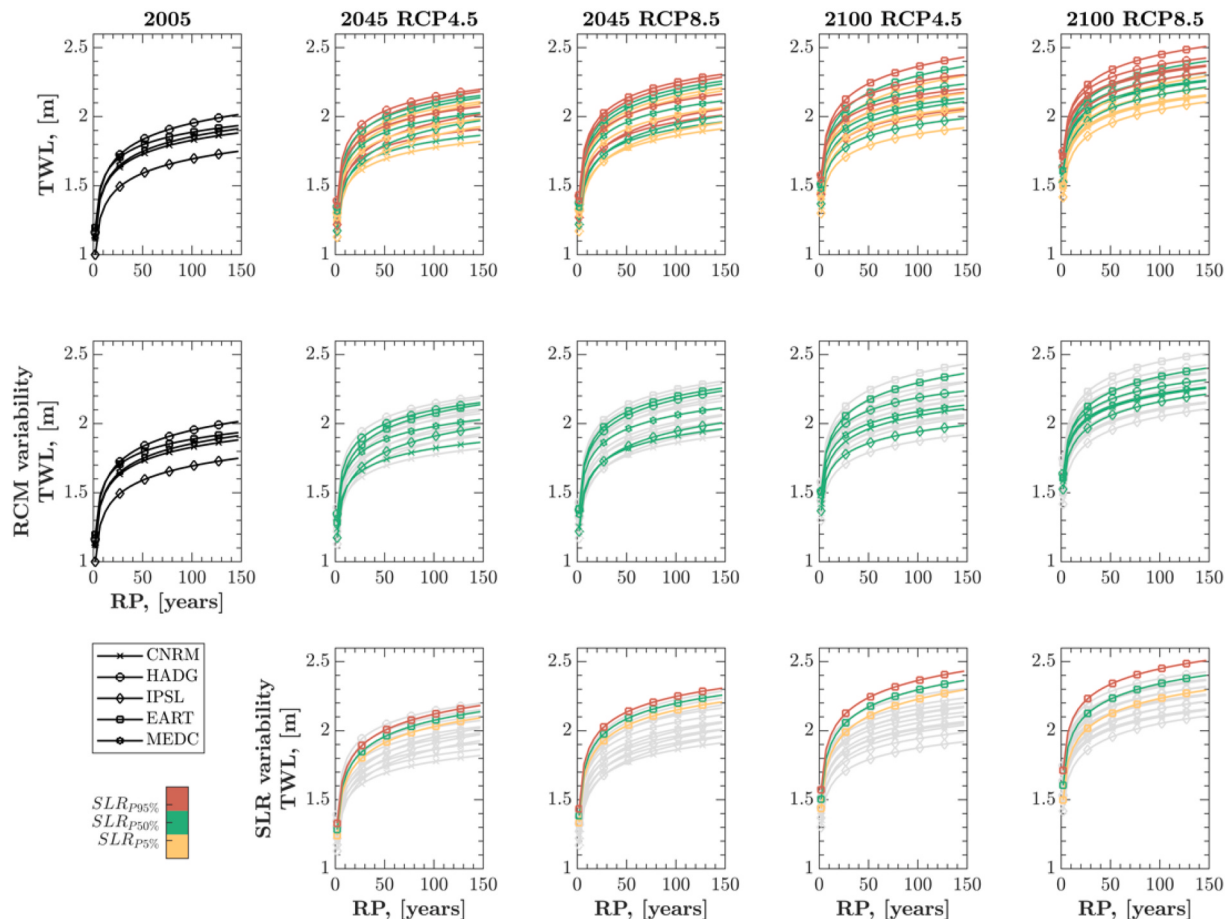


Fig. 8. PDFs of full-CA TWL in Almenara in 2005, 2045 and 2100 for the RCP4.5 and RCP8.5, where colour code refers to SLR percentiles and markers represent RCMs. The second and third row of panels illustrate the PDFs under RCM and SLR-percentile factorisations, respectively.

the shape of their profiles on which SLR and storms act. Almenara and Chilches have abrupt profiles but no major irregularities in the swash zone. The full CA for these beaches leads to the most dissipative profiles and the lowest TWL₁₀₀. With respect to the full CA in 2100, the short-term, long-term and no CAs provide, in relative terms, increased TWL₁₀₀ mean values by up to ~3%, ~4% and ~6% in Almenara and by up to ~2%, ~11% and ~17% in Chilches. The pattern in Burriana and Sagunto is different from that in Almenara and Chilches due to the presence of singularities in the profile swash zone. Storms acting above higher sea levels reach parts of the surveyed profiles with high jumps and flat areas, leading to non-linear changes in foreshore slope and affecting wave setup. In Burriana, the lowest TWL is reached with the short-term CA. With respect to the full CA, the short-term CA underestimates the TWL₁₀₀ mean values by ~5%–6%, and the long-term CA overestimates the TWL₁₀₀ mean values by ~4%–5%. In Sagunto, any CA other than the full CA underestimates the full CA TWL₁₀₀ mean value for any scenario and time horizon (~1%–7%), except for the long-term CA in 2100 due to SLR.

We also quantify the relative contributions of SLR percentiles, RCMs, and type of CA to TWL₁₀₀ total uncertainty by applying three-factor ANOVA-based variance decomposition (Storch and Zwiers, 1999). Fig. 10 presents the results for Burriana, Chilches, Almenara, and Sagunto in 2005, 2045, and 2100 for both RCP4.5 and RCP8.5, where the variance partitioning is compared considering the TWL obtained from all CAs. The findings are consistent with the results obtained in previous analyses. The SLR trajectory contribution (cyan) increases as we move farther away in time, and the radiative forcing becomes greater (from up to 11%, 5%, 9%, and 11% in 2045 to up to 35%, 23%, 55%, and 35% in 2100 in Burriana, Chilches, Almenara, and Sagunto,

respectively). RCM uncertainty governs in Burriana, Almenara and Sagunto in 2005 (~74%, ~80% and ~97, respectively), in 2045 (71–52%, 77–78% and 86–88%, respectively), and in 2100 for RCP4.5 (65%, 75% and 71%, respectively). We find a strong dominating influence of the CA in Chilches (~57%–68%), Burriana (~23%–36%) and Sagunto. Particularly in Sagunto, the CA contribution to TWL₁₀₀ total uncertainty starts to become noticeable in 2100 for RCP4.5 (~16%) and increases sharply for RCP8.5 (~46%), having even more weight than the SLR percentiles (~35%). Inter-CA variability is mainly related to the effect of foreshore slope changes on TWL. The greater the difference between the boxplots in Fig. 7, the more the CA affects TWL₁₀₀ uncertainty. Compared to that of other uncertainty sources, the contribution of pairwise and triple interactions (SLR–RCM, SLR–CA, RCM–CA, and SLR–RCM–CA) is negligible (<2%).

3.4. Effect of the coupling approach on coastal flooding

We apply the 2D flood model to obtain coastal flood maps driven by the TWL₁₀₀. In this step of the modelling chain, TB2020FULL/TB2020ST is replaced by TB2045FULL, TB2100FULL_RCP4.5 and TB2100FULL_RCP8.5 for the full CA and by TB2045ST, TB2100ST_RCP4.5 and TB2100ST_RCP8.5 for the short-term CA, which incorporate storm erosion (Table 4). For brevity, we denote the flooded area (FA) related to TWL₁₀₀ as FA₁₀₀ hereinafter.

Fig. 11 and Fig. 12 present some examples of the flood maps obtained. Fig. 11 shows the FA₁₀₀ maps in Moncofar and Corinto in 2045, factorised by CA and grouped by RCP. These maps correspond to the most unfavourable scenario considering the envelope of outcomes of the 5 RCMs and the SLR 95th percentile. In Moncofar, the full CA FA₁₀₀ may

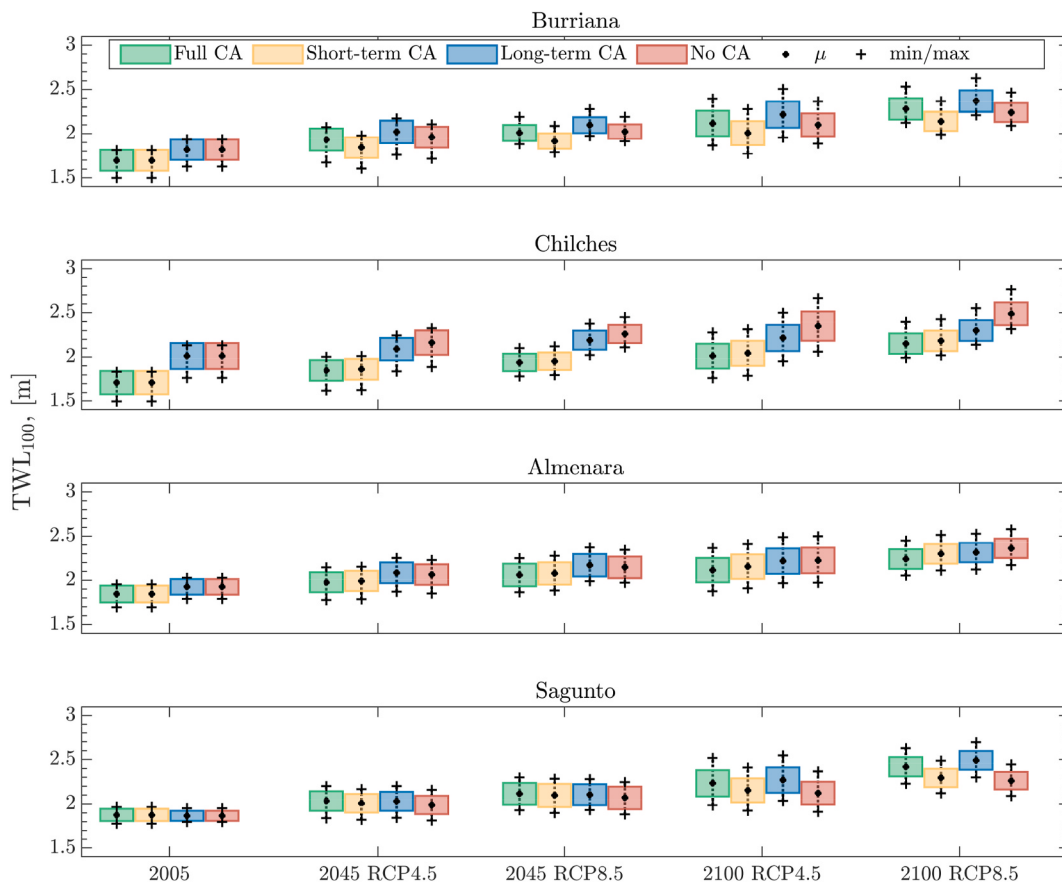


Fig. 9. TWL₁₀₀ value range in Burriana, Chilches, Almenara and Sagunto in 2005, 2045 and 2100 for the RCP4.5 and RCP8.5, where colour code refers to CA, black circles are mean values, crosses are maximum values and box limits represent mean values plus/minus deviations.

reach 44.92 ha on a beach reduced by 40% with respect to 2020 beach width. If long-term or no CA were instead applied, in relative terms, such FA could be overestimated by 40% and 22%, respectively. Long-term erosion represents a reduction in beach width of 19% with respect to 2020 beach width. The short-term CA, however, with 20% less beach width than in 2020, would underestimate FA₁₀₀ by 23% with respect to the full CA. This can be explained by the low importance of storm erosion on this beach due to the presence of groynes, in contrast to Corinto, where this percentage is reduced to 2%. In Corinto there is less erosion than in Moncofar. The full, long-term and short-term CAs account for 2020 beach width reduced by 33%, 9% and 14%, respectively. Fig. 12 shows FA₁₀₀ maps associated with each CA in Almenara in 2045 for RCP4.5 and the SLR 95th percentile factorised by RCM. From an uncertainty sampling point of view, the full and short-term CAs provide the widest and narrowest range of inter-RCM variation (15.19–27.32 ha and 15.97–22.96 ha), respectively. The worst-case RCM varies between CAs, with the EART model providing the largest FA₁₀₀ in the full CA (27.32 ha) and the HADG model for the short-term, long-term and no CAs (24.75 ha, 22.96 ha and 25.56 ha, respectively). In terms of erosion, the full CA reduces the 2020 beach width in Almenara by 27% while long-term and shor-term CAs do so by 16% and 11%, respectively.

As in the case of the TWL, we analyse the effect of CA choice on FA. Following the same examples of Burriana, Chilches, Almenara, and Sagunto, Fig. 13 shows FA₁₀₀ factorised by the CAs and grouped by time horizon and RCP. In 2005, the lower the TWL₁₀₀ the lower the FA₁₀₀, with a greater influence of the CA in FA₁₀₀ than in TWL₁₀₀. For instance, in Chilches and Almenara, long-term/no CA can provide overestimated TWL₁₀₀ mean values of approximately 17% and 5%, respectively, but underestimated FA₁₀₀ mean values of approximately 32% and 85%, respectively, in relative terms with respect to the full/short-term CA. In

contrast, in Burriana, the presence of groynes reduces the impact of storm erosion on FA₁₀₀. As time horizons move away, long-term topobathy changes due to SLR and longshore sediment transport increasingly contribute to the FA, leading to greater values and larger spread ranges. Regarding the influence of morphology on hydrodynamics, while the TWL is mainly affected by cross-shore transport (both short and long term), the FA is highly influenced by longshore-driven shoreline changes, which if they imply retreat, can in turn be enhanced by the long-term SLR landward and upward displacement and storm erosion, reducing protection services provided by the beaches. In contrast to TWL₁₀₀, the long-term CA provides the highest FA₁₀₀ values in almost every case because it is linked to high TWL₁₀₀ values and long-term shoreline changes, which are great contributors to flooding. On beaches such as Chilches, where there is a promenade that determines the evolution of the beach (especially in the long term), the higher the TWL is, the more overtopping and therefore the more coastal flooding there is. As such, the long-term and no CAs provide projected FA₁₀₀ mean values higher than those of the full CA by 36%–40% and 4%–18%, respectively. For mixed beaches such as Almenara or Sagunto, where only one part has a high degree of anthropisation and the rest is natural, the omission of flooding-erosion interplays can lead with respect to the full CA to either FA₁₀₀ overestimates of approximately 18%–22% (mean values) or underestimates of approximately 15%–16% (mean values) in 2050 and underestimates of up to 100% (22%–25% mean values) in 2100, in relative terms. Topobathy singularities (in both the swash zone and the land over which flood spreads) make it critical to consider the joint impact of erosion and flooding using surveyed profiles, as generalisations (e.g., standard correction factors) do not necessarily apply.

Fig. 14 allows visualisation of the relative contributions of SLR percentiles, RCMs and CAs to FA₁₀₀ total uncertainty for RCP4.5 and

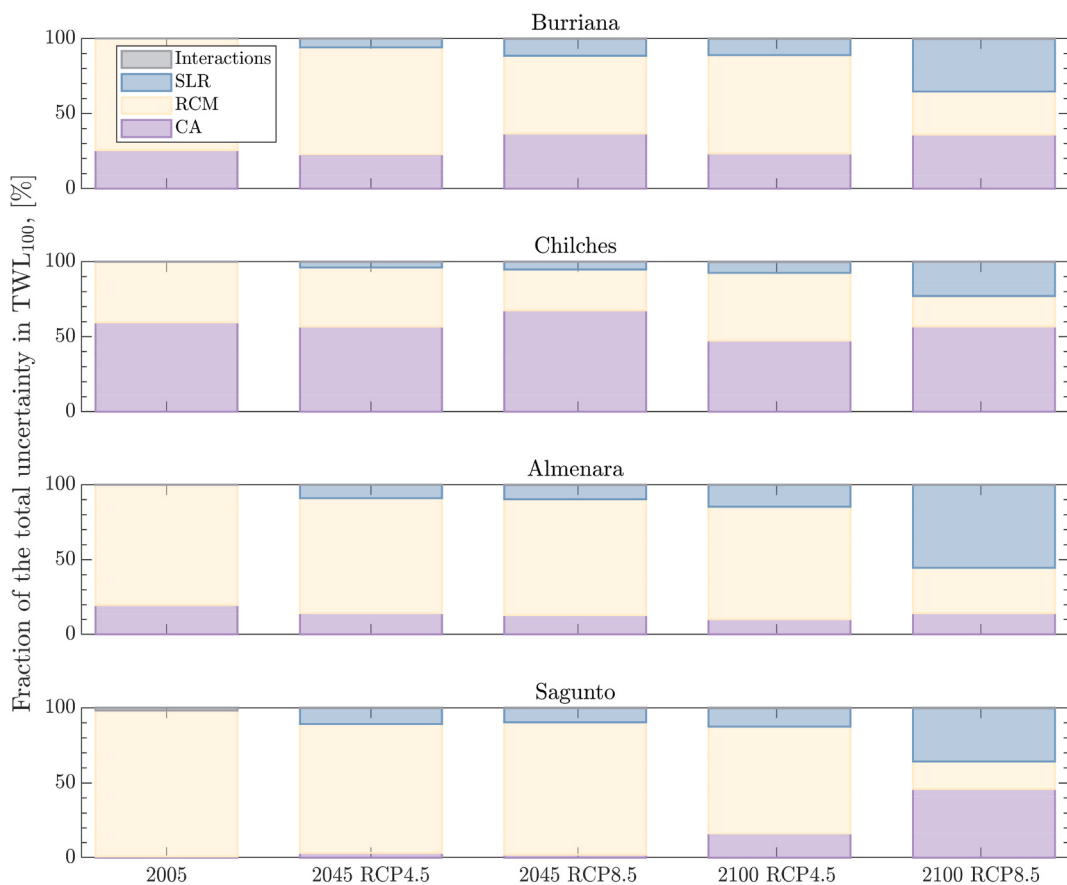


Fig. 10. Contribution of each uncertainty source and their interactions to total TWL₁₀₀ uncertainty.

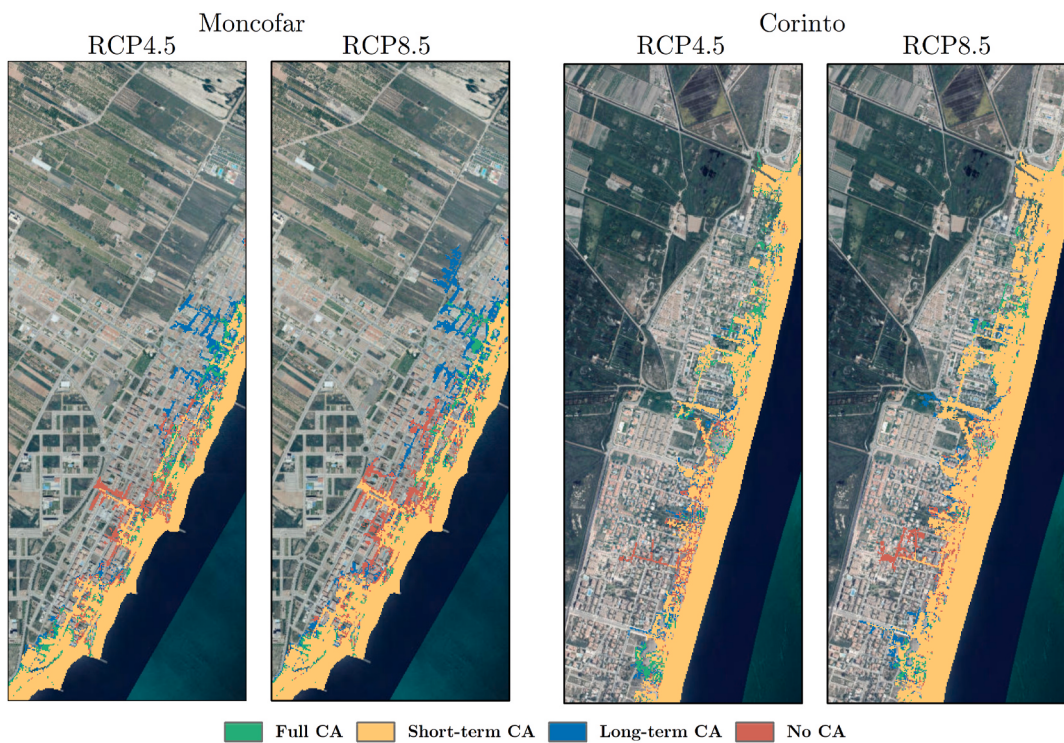


Fig. 11. FA₁₀₀ in Moncofar and Corinto in 2045 for the RCP4.5 and the RCP8.5, where the colour code refers to the four CA. Flood extents correspond to the envelope of RCMs and the SLR 95th percentile.

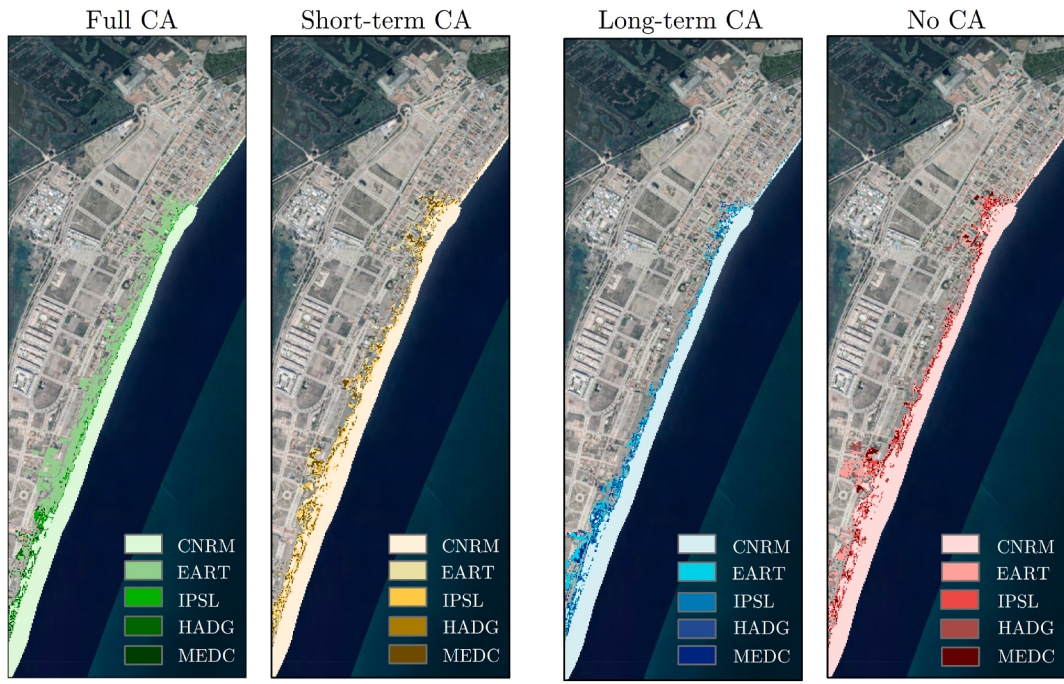


Fig. 12. FA₁₀₀ in Almenara in 2045 for the RCP4.5 and the SLR 95th percentile factorised by RCM (colour intensity).

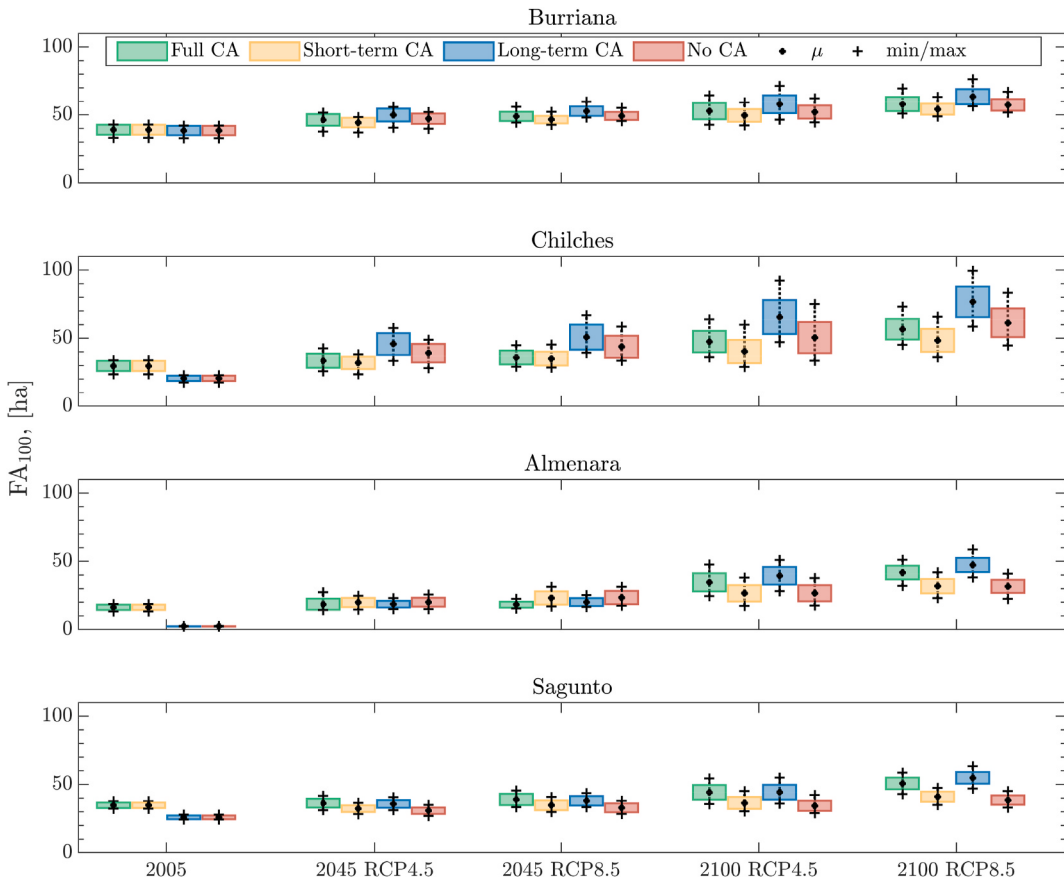


Fig. 13. FA₁₀₀ value range in Burriana, Chilches, Almenara and Sagunto in 2005, 2045 and 2100 for the RCP4.5 and RCP8.5, where colour code refers to CA, black circles are mean values, crosses are maximum values and box limits represent mean values plus/minus standard deviations.

RCP8.5 in 2005, 2045 and 2100. The SLR contribution in Burriana, Chilches, Almenara, and Sagunto increases for more distant time horizons and higher RCPs, although this effect is smaller for FA₁₀₀ (10–35%,

7–26%, 8–20% and 7–16% in 2100, respectively) than for TWL₁₀₀ (11–35%, 7–23%, 14–55% and 12–35% in 2100, respectively). The most striking aspect is the dominating influence of the CA on all these

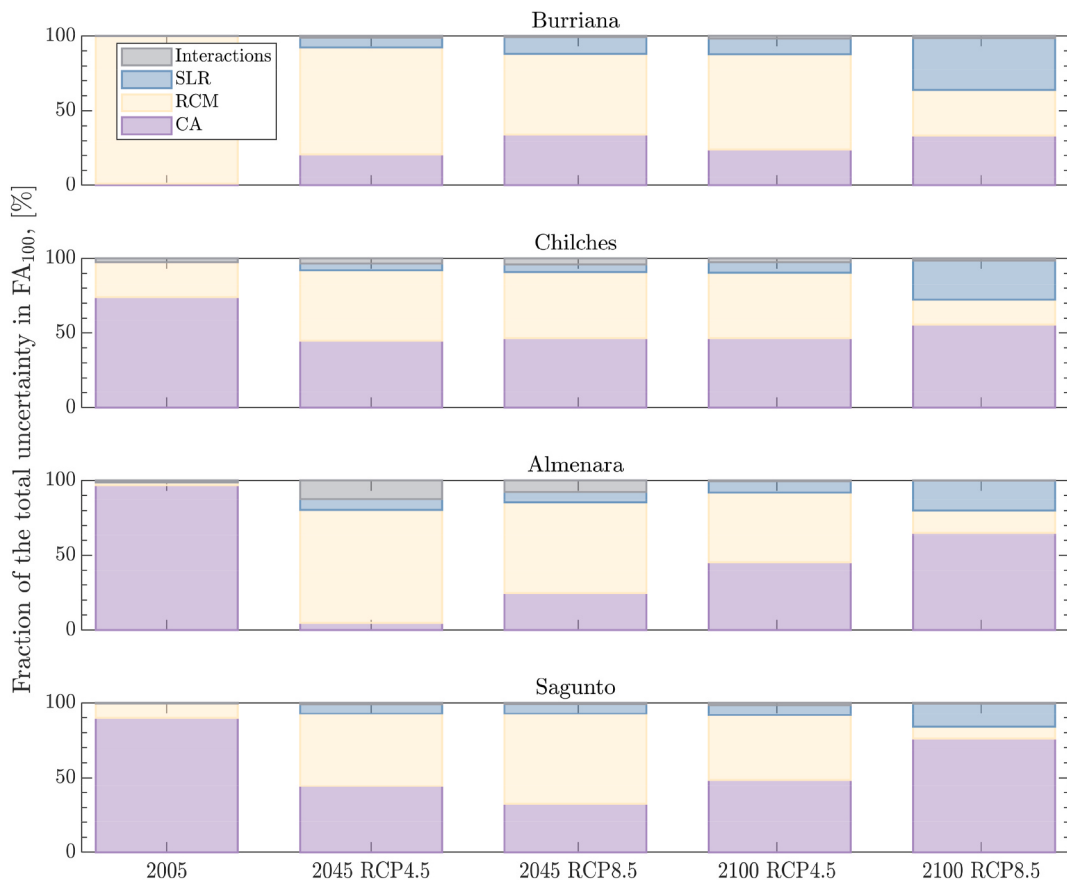


Fig. 14. Contribution of each uncertainty source and their interactions to total FA₁₀₀ uncertainty.

beaches, which is stronger than that of SLR percentiles in 2100 for RCP8.5 (~34%, ~56%, ~65% and ~76% of CA versus ~35%, ~26%, ~20% and ~16% of SLR, for Burriana, Chilches, Almenara and Sagunto, respectively). This highlights that no matter the efforts made to improve waves, storm surges and SLR projections, inaccuracies will occur if no appropriate coupling of flooding and erosion is considered. Inter-CA variability at the stage of inland flood modelling is partly inherited by TWL modelling but mostly attributed to the land part of the topobathies modified to account for long-term shoreline changes. It is also worth mentioning the contribution of RCM-CA interactions to FA₁₀₀ uncertainty in Chilches and Almenara in 2045 (up to 4% and 12%, respectively). This interplay has its origin in the TWL, as RCP-driven waves are scaled for each CA by foreshore slopes. Differences are small for TWL₁₀₀ but become larger in FA terms due to terrain heights (e.g., if water depth exceeds the height of a defence, flood extent can increase considerably if the area behind the structure has a low elevation level).

3.5. Summary of the main effects of the coupling approaches in coastal flood estimates

Although the numerical results presented above are site-specific, from the analyses we have identified patterns of how erosion and the coupling approach selected can influence the TWL and the FA that may be applicable to other beaches with similar characteristics.

Main effects on the TWL:

- In natural coastal areas, long-term processes do not necessarily lead to significant changes in the TWL. Longshore transport does not alter the profile shape, so the dissipation properties of natural profiles do not change. In idealised profiles, SLR would also have no influence on the TWL. The active profile would move upwards and landwards,

and the swash zone morphology facing the waves acting on top of higher sea level would be the same as without SLR. However, real profiles may show irregularities in the swash zone so that the SLR effect can change the TWL. The sign of these changes depends on the geometry of the profile.

- In anthropised coastal areas, long-term processes can lead to significant changes in the TWL. Profile changes due to longshore transport in squeezed coasts can induce local scour at the toe of the structure. SLR in front of undermined structures can reduce wave energy dissipation and increase overtopping rates.
- Coupling hydro- and morphodynamics during extreme events leads to lower TWL values than if a static profile is assumed. Cross-shore sediment transport from the beachface to the outer bar results in a more dissipative profile adapted to incoming wave conditions. As such, in most of the cases, the no and long-term CAs provide higher TWL values than the short-term and full CAs, which consider short-term profile adaptation.
- The relative contribution of the SLR percentile to the TWL increases with radiative forcing and time. RCM and CA influence the TWL significantly but their relative contribution is site-specific. The CA variance range is mainly given by changes in the foreshore slope. From our results, RCM uncertainty dominates over CA uncertainty except for the beach with the highest anthropisation level, where the relative contribution of the CA exceeds that of the rest of sources of uncertainty for any given scenario.

Main effects on the FA:

- In natural coastal areas, long-term processes can lead to significant changes on the FA. Longshore processes can generate sediment-starved regions, undermining the beachfront and decreasing flood

- protection. SLR-induced erosion and waves propagating on top of higher sea level reduce beach width and likely dune height.
- In anthropised coastal areas, the critical flood elevation is usually controlled by an artificial structure which is assumed to be non-erodible. Thus, the effects of long-term processes on coastal flooding are mainly due to more energetic waves reaching the coast as SLR increases and scouring progresses. From our results, considering longshore transport and SLR-induced erosion leads to higher FA than if these processes were not considered.
 - Short-term erosion can play a key role on the FA. In natural beaches, storm erosion results in two effects that can be counteracted. The foreshore slope is softened and the wave energy reaching the coast is reduced. The second effect is the beachface and dune crest decrease. While the first effect causes the TWL to decrease, the FA can increase or decrease relative to the no CA depending on the magnitude of the storm erosion and the condition of the beach when that storm occurs. From our results, considering storm erosion overall provides lower FA than if it were neglected. The effect of TWL reduction due to wave dissipation is greater than that of short-term erosion in the FA, but this might not be the case in other sites or under different assumptions. Two factors can influence this outcome. For this application, we used two different models to account for short-term erosion in the TWL and the FA. These two models can have different sensitivity and provide different erosion volumes, even for the same storm. While this may affect the magnitude of the result, we have found that it does not affect the signal and that our conclusions are robust regardless of the model chosen (see Supplementary Material for details). The other factor is related to the limitations of the probabilistic approach, since we do not know the storm erosion corresponding to the TWL₁₀₀ that we used as flood forcing. Instead, we eroded each beach over which we modelled flooding considering an average storm, a more centred statistic than the TWL₁₀₀.
 - The relative contribution of the SLR percentile to the FA increases with radiative forcing and time, but to a lesser extent than for the TWL. The CA has a dominating influence on the FA in most of the beaches, which can exceed that of the RCMs and SLR percentiles even for the highest radiative forcing in 2100. The CA variance range is partly inherited by that of the TWL (and thus by changes in the foreshore slope) but mostly attributed to considering or not long-term shoreline changes in the coastal flood modelling. The FA largely depends on terrain heights.

4. Conclusions

Reliable coastal flood projections are essential for coastal management planning and climate change adaptation. However, their development remains a challenge in several ways. Coastal flooding does not occur in isolation but is the result of the interaction of complex hydrodynamic and morphodynamic processes at different time scales (hours to decades), which makes it difficult to analyse them jointly. In addition, decision-making in this context takes place at the regional level and requires sufficient consideration of uncertainty. Such uncertainty arises from the choice of radiative forcing scenarios, climate models and mean sea-level rise trajectories, growing with timescale (up to centuries), as well as from the flood projection modelling process itself, and need to be adequately sampled.

In this paper, we present a methodology to develop coastal flood projections combined with coastal erosion that, with respect to the published literature, combines a set of elements in a novel way and improves both the coupling of coastal flooding and erosion at the relevant scales (short and long term) and the consideration of uncertainty. We apply a suite of statistical, process-based, and physics-based models to regionally generate and downscale synthetic storms, compute hydrodynamics and morphodynamics, elaborate future topo-bathymetries incorporating long-term shoreline changes and storm erosion, and model coastal flood propagation inland. As climate forcing conditions,

we use multi-model projected nearshore waves, storm surges and mean sea-level rise. To sample their associated knowledge-based and intrinsic uncertainty, we consider two representative concentration pathways, five configurations of global and regional climate models, three trajectories of mean sea-level rise, and thousands of synthetic multivariate storms. The aim of using synthetic storms is to consider the complete range of combinations of the projected climate variables that can cause coastal flooding. This is key since the dynamic projections of wave conditions and storm surges (a single realisation per radiative forcing scenario and configuration of climate models) do not necessarily contain the highest possible values of the individual variables or combinations of these variables that maximise total water levels. As a result, we present total water levels and flooded areas in 2050 and 2100.

We analyse for the first time how different levels of flooding and erosion coupling can influence coastal flood-related estimates. The results show that considering short- and long-term coupling (full coupling), short- or long-term coupling alone, or no coupling (the standard approach) can lead to important differences in total water levels, and especially in the flooded area. The factors that most influence total water levels are short-term erosion (making profiles more dissipative and reducing their value) and profile geometry. Furthermore, changes to the shape of the beach profile determine whether sea-level rise reduces or increases the wave contribution to the total water level. In the flooded area, however, longshore transport-driven long-term erosion plays a fundamental enhancing role. The contribution of storm erosion is also important, but as we move forward in time and for higher radiative forcing scenarios, its effect is outweighed by longshore transport-driven long-term erosion and the effect of sea-level rise. These patterns are in turn conditioned by the real-world distribution of terrain heights. As such, the standard approach could yield mean values of water levels and flooded land surfaces that are overestimated by 18% and 22%, respectively, or underestimated by 7% and 85%, respectively, in 2100 with respect to those from the full coupling approach. Based on the degree of anthropisation of the coast and how this determines beach evolution over time, incomplete coupling approaches could lead to mean values of flooded area that are overestimated or underestimated by up to 40% and 25%, respectively, with respect to the proposed approach. These biases could lead to misidentification of priorities for adaptation or failure to appropriately allocate adaptation funds in terms of location, amount, and timing.

We also examine how the coupling approach and other uncertainty sources can contribute to the variance of the results. In terms of total water level, the relative importance of the coupling approach highly depends on the profile geometry, ranging from ~1% to ~68% in 2045 and from ~10% to ~57% in 2100. For the remaining uncertainty factors, the selection of climate models dominates that of sea level rise trajectories in all scenarios and time horizons except for the highest radiative forcing scenario in 2100. In terms of the flooded area, the influence of the choice of the coupling approach on the results is greater than for the total water level, and it can become dominant over that of climate models and sea-level rise trajectories (up to 76% versus 8% and 16%, respectively), even by 2100. This means that even the best projections of storm surges, waves and sea-level rise could provide spurious projections of flooded areas if shoreline changes are not properly accounted for in the topo-bathymetry. Overall, inter-coupling approach variability can be partly attributed to foreshore slope changes along the swash zone of beach profiles (due to smoothing of the slope caused by storms and sea-level rise) and partly to the long-term translation of the land portion of the topo-bathymetries over which inland flooding spreads, in any case highlighting the relevance of employing real profiles rather than theoretical profiles for solving volume conservation and shoreface translation.

Our approach to consider erosion-enhanced flooding at the climate change scale has potential for improvement. First, the simple translation rules that we applied to upscale the shoreline movement to a two-dimensional topo-bathymetry are a simplification of reality. The

availability of observations to calibrate profile translation models would allow more accurate results to be obtained. Second, the representative storm erosion events that we used for the short-term topo-bathymetry update did not correspond to any total water level flood forcing condition but were obtained from IH-LANS as a proxy allowing for a compromise solution given the probabilistic nature of the study. We considered an average storm erosion which presumably leads to an underestimation of the flooded area in relation to the storm erosion we would have obtained with XBeach. Although at a high computational cost, it is worth investigating how to establish a realistic relationship between XBeach morphodynamic changes and the 100-year total water level, calculated probabilistically based on thousands of storms hybrily downscaled using XBeach and statistical tools. Third, for the short-term topo-bathymetry update, we assumed that the beach has receded due to long-term processes (in the coupling approaches that consider this to be the case) but not due to a previous storm. The consideration of the effect of storm clusters would allow the analysis of a situation of extreme erosion, which will become more frequent with climate change, providing new information to establish general rules of behaviour. Finally, in this study we present an approach for modelling the effect of short- and long-term erosion on coastal flooding. This approach was calibrated at present, considering only the short-term component. This implies that we assumed that the present calibration is valid for the future, which is not necessarily the case. Moreover, considering new processes into future projections may incorporate additional uncertainty. Future developments of this research work would therefore benefit from systematic long-term monitoring of shoreline changes and flooding.

CRediT authorship contribution statement

A. Toimil: Conceptualization, Methodology, Software, Formal analysis, Writing – original draft, Project administration, Funding acquisition. **M. Álvarez-Cuesta:** Methodology, Software, Validation, Formal analysis, Visualization, Writing – review & editing. **I.J. Losada:** Conceptualization, Methodology, Writing – review & editing, Project administration, Funding acquisition.

Declaration of competing interest

The authors declare that they have no known competing financial interests or personal relationships that could have appeared to influence the work reported in this paper.

Data availability

Data will be made available on request.

Acknowledgments

This study was partially funded by the Spanish Government through the grant COASTALfutures (PID2021-126506OB-100); the Government of Cantabria through the FENIX Project; and the European Union's Horizon 2020 CoCliCo Project (grant agreement No 101003598). AT and MA-C are also funded by the Spanish Ministry of Science and Innovation through the Ramon y Cajal Programme (RYC2021-030873-I) and the FPI studentship (PRE-2018-085009), respectively.

Appendix A. Supplementary data

Supplementary data to this article can be found online at <https://doi.org/10.1016/j.coastaleng.2022.104248>.

References

- Álvarez-Cuesta, M., Toimil, A., Losada, I.J., 2021a. Modelling long-term shoreline evolution in highly anthropized coastal areas. Part 1: model description and validation. *Coast. Eng.* 169, 103960.
- Álvarez-Cuesta, M., Toimil, A., Losada, I.J., 2021b. Modelling long-term shoreline evolution in highly anthropized coastal areas. Part 2: assessing the response to climate change. *Coast. Eng.* 168, 103961.
- Antolínez, J.A., Méndez, F.J., Anderson, D., Ruggiero, P., Kaminsky, G.M., 2019. Predicting climate-driven coastlines with a simple and efficient multiscale model. *J. Geophys. Res.: Earth Surf.* 124 (6), 1596–1624.
- Arns, A., Dangendorf, S., Jensen, J., Tallek, S., Bender, J., Charitha, P., 2017. Sea-level rise induced amplification of coastal protection design heights. *Sci. Rep.* 7, 40171.
- Barnard, P.L., Erikson, L.H., Foxgrover, A.C., Finzi Hart, J.A., Limber, P., O'Neil, A.C., van Ormondt, M., Vitousek, S., Wood, N., Hayden, M.K., Jones, J.M., 2019. Dynamic flood modelling essential to assess the coastal impacts of climate change. *Sci. Rep.* 9, 4309.
- Bates, P.D., De Roo, A.P.J., 2000. A simple raster-based model for floodplain inundation. *J. Hydrol.* 236, 54–77.
- Benavente, J., Del Rio, L., Gracia, F.J., Martínez-del-Pozo, 2006. Coastal flooding hazard related to storms and coastal evolution in Valdelagrana spit (Cádiz Bay Natural Park, SW Spain). *Continent. Shelf Res.* 26, 1061–1076.
- Booij, N., Ris, R.C., Holthuijsen, L.H., 1999. A third-generation wave model for coastal regions 1. Model description and validation. *J. Geophys. Res. Oceans* 104, 7649–7666.
- Bruun, P., 1962. Sea-level rise as a cause of shore erosion. *J. Waterw. Harb. Div. ASCE* 88, 117–130.
- Camus, P., Mendez, F.J., Medina, R., 2011. A hybrid efficient method to downscale wave climate to Coastal areas. *Coast. Eng.* 58, 851–862.
- Cazenave, A., Le Cozannet, G., 2013. Sea level rise and its coastal impacts. *Earth's Future* 2, 15–34.
- Collins, M., Sutherland, M., Bouwer, L., Cheong, S.-M., Fröhlicher, T., Jacot Des Combes, H., Roxy, M. Koll, Ij Losada, K. McInnes, Ratter, B., Rivera-Arriaga, E., Susanto, R.D., Swingedouw, D., Tibig, L., 2019. Extremes, abrupt changes and managing risk. In: Pörtner, H.-O., et al. (Eds.), *IPCC Special Report on the Ocean and Cryosphere in a Changing Climate (SROCC)*.
- Dawson, R.J., Dickson, M.E., Nicholls, R.J., et al., 2009. Integrated analysis of risks of coastal flooding and cliff erosion under scenarios of long-term change. *Clim. Change* 95, 249–288.
- Dean, R.G., 1991. Equilibrium beach profiles: characteristics and applications. *J. Coast Res.* 7 (1), 53–84.
- Egbert, G.D., Erofeeva, S.Y., 2002. Efficient inverse modeling of barotropic ocean tides. *J. Atmos. Ocean. Technol.* 19 (2), 183–204.
- Erikson, L.H., O'Neill, A., Barnard, P.L., Vitousek, S., Limber, P., 2017. Climate change-driven cliff and beach evolution at decadal to centennial time scales. *Coast. Dynam.* 210, 125–136. 2017 Paper No.
- Fang, N.F., Shi, Z.H., Yue, B.J., Wang, L., 2013. The characteristics of extreme erosion events in a small mountainous watershed. *PLoS One* 8 (10), e76610.
- Fox-Kemper, B., Hewitt, H.T., Xiao, C., Ádalgeirsdóttir, G., Drijfhout, S.S., Edwards, T.L., Golledge, N.R., Hemer, M., Kopp, R.E., Krinner, G., Mix, A., Notz, D., Nowicki, S., Nurhati, I.S., Ruiz, L., Sallée, J.-B., Aba, Slanger, Yu, Y., 2021. Ocean, cryosphere and sea level change. In: *Climate Change 2021: The Physical Science Basis. Contribution of Working Group I to the Sixth Assessment Report of the Intergovernmental Panel on Climate Change* [Masson-Delmotte VP et al. Cambridge University Press (Press)].
- Gharagozlou, A., Dietrich, J.C., Karancı, A., Luettich, R.A., Overton, M.F., 2020. Storm-driven erosion and inundation of barrier islands from dune-to-region-scales. *Coast. Eng.* 158, 103674.
- Gomes da Silva, P., Coco, G., Garnier, R., Klein, A.H.F., 2020. On the prediction of runup, setup and swash on beaches. *Earth Sci. Rev.* 2014, 103148.
- Gouldby, B.P., Sayers, P.B., Panzeri, M.C., Lanyon, J.E., 2010. Development and application of efficient methods for the forward propagation of epistemic uncertainty and sensitivity analysis within complex broad-scale flood risk system models. *Can. J. Civ. Eng.* 37 (7), 955–967.
- Gouldby, B.P., Sayers, P.B., Mulet-Martí, J., Hassan, M., Benwell, D., 2008. A methodology for regional scale flood risk assessment. *Water Manag.* 161 (3), 2008.
- Grases, A., Gracia, V., García-León, M., Lin-Ye, J., Sierra, J.P., 2020. Coastal flooding and erosion under a changing climate: implications at a low-lying coast (Ebro Delta). *Water* 12, 346.
- Grilli, A., Spaulding, M.L., Oakley, B.A., Damon, C., 2017. Mapping the coastal risk for the next century, including sea level rise and changes in the coastline: application to Charlestown RI, USA. *Nat. Hazards* 88, 389–414.
- Gutierrez, B.T., Plant, N.G., Pendleton, E.A., Thieler, E.R., 2014. Using a Bayesian Network to Predict Shoreline Change Vulnerability to Sea Level Rise for the Coasts of the United States. Rep. U.S. Geol. Surv. Open-File Rep. 2014-1083, p. 26.
- IHCantabria, 2020. High-Resolution Projections of Waves and Water Levels along the Spanish Coast. in Spanish. Spanish Ministry for the Ecological Transition and the Demographic Challenge, p. 60. July 2021. <https://www.miteco.gob.es/es/costas/temas/proteccion-costa/estrategia-adaptacion-cambio-climatico/default.aspx>.
- Jamieson, S., L'homme, J., Wright, G., Gouldby, B., 2012. Highly efficient 2D inundation modelling with enhanced diffusion-wave and sub-element topography. *Proc. Inst. Wat. Man.* 165 (10), 581–595.
- Kinsela, M.A., Morris, B.D., Linklater, M., Hanslow, D.J., 2017. Second-pass assessment of potential exposure to shoreline change in New South Wales, Australia, using a sediment compartments framework. *J. Mar. Sci. Eng.* 5 (4), 61.

- Leaman, C.K., Harley, M.D., Splinter, K.D., Thran, M.C., Kinsela, M.A., Turner, I.L., 2021. A storm hazard matrix combining coastal flooding and beach erosion. *Coast. Eng.* 170, 104001.
- Lentz, E.E., Thieler, E.R., Plant, N.G., Stippa, S.R., Horton, R.M., Gesch, D.B., 2016. Evaluation of dynamic coastal response to sea-level rise modifies inundation likelihood. *Nat. Clim. Change* 6 (7), 696–700.
- Limber, P.W., Barnard, P.L., Vitousek, S., Erikson, L.H., 2018. A model ensemble for projecting multidecadal coastal cliff retreat during the 21st century. *J. Geophys. Res. Earth Surface* 123, 1556–1589.
- Lin-Ye, J., García-Leon, M., Gracia, V., Ortego, M.I., Lionello, P., Sanchez-Arcilla, A., 2017. Multivariate statistical modelling of future marine storms. *Appl. Ocean Res.* 65, 192–205.
- Lobeto, H., Menendez, M., Losada, I.J., 2021. Future behavior of wind wave extremes due to climate change. *Sci. Rep.* 11 (1), 1–12.
- Lucio, D., Tomas, A., Lara, J.L., Camus, P., Losada, I.J., 2020. Stochastic modelling of long-term wave climate based on weather patterns for coastal structures applications. *Coast. Eng.* 161, 103771.
- Luettich, R.A., Westerink, J.J., Scheffner, N.W., 1992. ADCIRC: an advanced three-dimensional circulation model for shelves coasts and Estuaries, *report 1: Theory and Methodology of ADCIRC-2DDI and ADCIRC-3DL*. United States army corps of Engineers. Tech. rep.
- Marcos, M., Tsimplis, M.N., Shaw, A.G.P., 2009. Sea level extremes in southern Europe. *J. Geophys. Res. Oceans* 114, C01007.
- Mardia, K.V., 1975. Statistics of directional data. *J. Roy. Stat. Soc. B* 37 (3), 349–371.
- Mardia, K.V., Hughes, G., Taylor, C.C., Singh, H., 2008a. A multivariate von Mises distribution with applications to bioinformatics. *Can. J. Stat.* 36 (1), 99–109. <https://doi.org/10.1002/cjs.5550360110>.
- Mardia, K.V., Hughes, G., Taylor, C.C., Singh, H., 2008b. A multivariate von Mises distribution with applications to bioinformatics. *Can. J. Stat.* 36 (1), 99–109.
- McCall, R.T., Van Thiel de Vries, J.S.M., Plant, N.G., Van Dongeren, A.R., Roelvink, J.A., Thompson, D.M., Reniers, A.J.H.M., 2010. Two-dimensional time dependent hurricane overwash and erosion modeling at Santa Rosa Island. *Coast. Eng.* 57, 668–683.
- McCarroll, R.J., Masselink, G., Valiente, N.G., Scott, T., Wiggins, M., Kirby, J.-A., Davidson, M., 2021. A rules-based shoreface translation and sediment budgeting tool for estimating coastal change: ShoreTrans. *Mar. Geol.* 435, 106466.
- Menendez, P., Losada, I.J., Torres-Ortega, S., Toimil, A., Beck, M.W., 2019. Assessing the effects of using high-quality data and high-resolution models in valuing flood protection services of mangroves. *PLoS One* 14 (8), e0220941.
- Miller, J.K., Dean, R.G., 2004. A simple new shoreline change model. *Coast. Eng.* 51 (7), 531–556.
- Milly, P.C.D., Wetherald, R.T., Dunne, K.A., Delworth, T.L., 2002. Increasing risk of great floods in a changing climate. *Nature* 415, 514–517.
- Montaño, J., Coco, G., Antolínez, J.A., Beuken, T., Bryan, K.R., Cagigal, L., et al., 2020. Blind testing of shoreline evolution models. *Sci. Rep.* 10 (1), 1–10.
- Nicholls, R.J., Cazenave, A., 2010. Sea-level rise and its impact on coastal zone. *Science* 328 (5985), 1517–1520.
- Oppenheimer, M., Glacovic, B., Hinkel, J., Van De Wal, R., Magnan, A., Abd-Elgawad, A., Cai, R., Cifuentes-Jara, M., Deconto, R., Ghosh, T., Hay, J., Isla, F., Marzeion, B., Meyssignac, M., Sebesvari, Z., 2019. Sea-level Rise and Implications for Low Lying Islands. Coasts and Communities, Special Report on the Ocean, and Cryosphere in a Changing Climate (SROCC).
- Passeri, D.L., Hagen, S.C., Bilskie, M.V., Madeiros, S.C., 2015. On the significance of incorporating shoreline changes for evaluating coastal hydrodynamics under sea level rise scenarios. *Nat. Hazards* 75, 1599–1617.
- Passeri, D.L., Hagen, S.C., Plant, N.G., Bilskie, M.V., Medeiros, S.C., Alizad, K., 2016. Tidal hydrodynamics under future sea level rise and coastal morphology in the Northern Gulf of Mexico. *Earth's Future* 4, 159–176.
- Passeri, D.L., Bilskie, M.V., Plant, N.G., Long, J.W., Hagen, S.C., 2018. Dynamic modelling of barrier island response to hurricane storm surge under future sea level rise. *Clim. Change* 149, 413–425.
- Pollard, J.A., Spencer, T., Brooks, S.M., 2019. *Prog. Phys. Geogr.* 43 (4), 574–585.
- Ranasinghe, R., 2016. Assessing climate change impacts on open sandy coasts: a review. *Earth Sci. Rev.* 160, 320–332.
- Ranasinghe, R., 2020. On the need for a new generation of coastal change models for the 21st century. *Sci. Rep.* 10 (1), 1–6.
- Roelvink, D., Reniers, A., van Dongeren, A., van Thiel de Vries, J., McCall, R., Lescinski, J., 2009. Modelling storm impacts on beaches, dunes, and barrier islands. *Coast. Eng.* 56, 1133–1152.
- Sanuy, M., Jimenez, J.A., 2021. Probabilistic characterisation of coastal storm-induced risks using Bayesian networks. *Nat. Hazards Earth Syst. Sci.* 21, 219–238.
- Sanuy, M., Jimenez, J.A., Ortego, M.I., Toimil, A., 2019. Differences in assigning probabilities to coastal inundation hazard estimators: event versus response approach. *J. Flood Risk Management*, e12557.
- Sayol, J.M., Marcos, M., 2018. Assessing flood risk under sea level rise and extreme sea levels scenarios: application to the Ebro Delta. *J. Geophys. Res. Oceans* 123 (2), 794–811.
- Sherwood, C.R., Van Dongeren, A., Doyle, J., Hegermiller, C.A., Hsu, T.J., Kalra, T.S., et al., 2022. Modeling the morphodynamics of coastal responses to extreme events: what shape are we in? *Ann. Rev. Mar. Sci.* 14, 457–492.
- Shchepetkin, A.F., McWilliams, J.C., 2005. The regional oceanic modeling system (ROMS): a split-explicit, free-surface, topography-following-coordinate oceanic model. *Ocean Model.* 9, 347–404.
- Splinter, K.D., Coco, G., 2021. Challenges and opportunities in coastal shoreline prediction. *Front. Mar. Sci.* <https://doi.org/10.3389/fmars.2021.788657>.
- Stockdon, H.F., Holman, R.A., Howd, P.A., Ahjr, Sallenger, 2006. Empirical parameterization of setup, Swash, and Runup. *Coast. Eng.* 53, 573–588.
- Storch, H.V., Zwiers, F.W., 1999. *Statistical Analysis in Climate Research*. Cambridge Univ. Press.
- Stripling, S., Panzeri, M., Blanco, B., Rossington, K., Sayers, P., Borthwick, A., 2017. Regional-scale probabilistic shoreline evolution modelling for flood risk assessment. *Coast. Eng.* 121, 129–144.
- Tebaldi, C., Ranasinghe, R., Voudoukakas, M., Rasmussen, D.J., Vega-Westhoff, B., Kireci, E., Mentaschi, L., 2021. Extreme sea-levels at different global warming levels. *Nat. Clim. Change* 1–6.
- Toimil, A., Camus, P., Losada, I.J., Alvarez-Cuesta, M., 2021. Visualising the uncertainty cascade in multi-ensemble probabilistic coastal erosion projections. *Front. Mar. Sci.* 8, 683535.
- Toimil, A., Losada, I.J., Nicholls, R.J., Dalrymple, R.A., Stive, M.J.F., 2020a. Addressing the challenges of climate change risks and adaptation in coastal areas: a review. *Coast. Eng.* 156, 103611.
- Toimil, A., Camus, P., Losada, I.J., Le Cozannet, G., Nicholls, R.J., Idier, D., Maspataud, A., 2020b. Climate change-driven coastal erosion modelling in temperate sandy beaches: methods and uncertainty treatment. *Earth Sci. Rev.* 202, 103110.
- Toimil, A., Losada, I.J., Diaz-Simal, P., Izaguirre, C., Camus, P., 2017a. Multi-sectoral, high-resolution assessment of climate change consequences of coastal flooding. *Clim. Change* 145, 431–444.
- Toimil, A., Losada, I.J., Camus, P., Diaz-Simal, P., 2017b. Managing coastal erosion under climate change at the regional scale. *Coast. Eng.* 128 (August), 106–122.
- Tolman, H., The WaveWatch III® Development Group, 2014. User Manual and System Documentation of WAVEWATCH III® Version 4.18. Tech. Note 316, NOAA/NWS/NCEP/MMAB. U.S. Department of Commerce, National Oceanic and Atmospheric Administration, National Weather Service, National Centers for Environmental Prediction, University Research Court College Park, Maryland, 282.
- USACE, 1984. Shore Protection Manual, Waterways Experiment Station , Corps of Engineers. Department of the Army, Waterways Experiment Station, 1, II.
- Van Ormondt, M., Nelson, T.R., Hapke, C.I., Roelvink, D., 2020. Morphodynamic modelling of the wilderness breach, Fire Island, New York. Part I: model set-up and validation. *Coast. Eng.* 157, 103624.
- Vitousek, S., Barnard, P.L., Limber, P., 2017a. Can beaches survive climate change? *J. Geophys. Res.: Earth Surf.* 122 (4), 1060–1067. <https://doi.org/10.1002/2017JF004308>.
- Vitousek, S., Barnard, P.L., Limber, P., Erikson, L., Cole, B., 2017b. A model integrating longshore and cross-shore processes for predicting long-term shoreline response to climate change. *J. Geophys. Res.: Earth Surf.* 122 (4), 782–806.
- Vos, K., Splinter, K.D., Harley, M.D., Simmons, J.A., Turner, I.L., 2019. CoastSat: a Google Earth Engine-enabled Python toolkit to extract shorelines from publicly available satellite imagery. *Environ. Model. Software* 122, 104528.
- Wahl, T., Plant, N.G., Long, J.W., 2016. Probabilistic assessment of erosion and flooding risk in the northern Gulf of Mexico. *J. Geophys. Res. Oceans* 121, 3029–3043.
- Walkden, M.J.A., Hall, J.W., 2005. A predictive mesoscale model of the erosion and profile development of soft rock shores. *Coast. Eng.* 52, 535–563.
- Wong, P.P., Losada, I.J., Gattuso, J.P., Hinkel, J., Khattabi, A., McInnes, K.L., Saito, Y., Sallenger, A., 2014. Coastal systems and low-lying areas. In: Field, C.B. (Ed.), *Climate Change 2014: Impacts, Adaptation, and Vulnerability; Part A: Global and Sectoral Aspects*. Contribution of Working Group II to the Fifth Assessment Report of the Intergovernmental Panel on Climate Change. Cambridge University Press, Cambridge, UK; New York, NY, USA, pp. 361–409.
- Zscheischler, J., Westra, S., van den Hurk, B.J.M., Seneviratne, S.I., Ward, P.J., Pitman, A., AghaKouchak, A., Bresch, D.N., Leonard, M., Wahl, T., Zhang, X., 2018. Future climate risk from compound events. *Nat. Clim. Change* 8, 469–477.